THE FLORIDA STATE UNIVERSITY

COLLEGE OF ARTS AND SCIENCES

CIRCULATION DYNAMICS AND LARVAL TRANSPORT MECHANISMS IN THE FLORIDA BIG BEND

By

AUSTIN C. TODD

A Dissertation submitted to the
Department of Earth, Ocean and Atmospheric Science
in partial fulfillment of the
requirements for the degree of
Doctor of Philosphy

Degree Awarded:
Spring Semester, 2013

Austin C. Todd defended this dissertation on February 1, 2013.

The members of the supervisory committee were:

Eric Chassignet
Professor Directing Dissertation

Mark Bourassa
University Representative

Allan Clarke
Committee Member

Felicia Coleman
Committee Member

William Dewar
Committee Member

Markus Heuttel
Committee Member

Steven Morey
Committee Member

The Graduate School has verified and approved the above-named committee members, and certifies that the dissertation has been approved in accordance with the university requirements.

TABLE OF CONTENTS

LIST OF TABLES

LIST OF FIGURES

LIST OF ABBREVIATIONS

ADCP	Acoustic Doppler current profiler
AWAC	Acoustic wave and current
BBR	Big Bend region
BBROMS	Big Bend regional ocean modeling system
CFSR	Climate System Forecast Reanalysis
COAMPS	Coupled Ocean / Atmosphere Mesoscale Prediction System
CSB	Cape San Blas
CSG	Cape St. George
DEM	Digital Elevation Model
ENSO	El Niño / Southern Oscillation
FPS	Florida Panhandle Shelf
GODAE	Global Ocean Data Assimilation Experiment
GOM	Gulf of Mexico
HYCOM	Hybrid Coordinate Ocean Model
IQR	Interquartile range
LC	Loop Current
LTRANS	Larval transport Lagrangian model
MISST	Multi-sensor improved sea surface temperature
MPDATA	Multidimensional positive definite advection transport algorithm
MSMR	Madison Swanson Marine Reserve
NARR	North American Regional Reanalysis
NCEP	National Center for Environmental Prediction
NCODA	Navy Coupled Ocean Data Assimilation
NDBC	National Data Buoy Center
NEGOM	Northeastern Gulf of Mexico
NGDC	National Geophysical Data Center
NOAA	National Oceanic and Atmospheric Administration
NOGAPS	Navy Operational Global Atmospheric Prediction System
NRL	Naval Research Laboratory
PLD	Pelagic larval duration
PV	Potential vorticity
ROMS	Regional ocean modeling system
rmse	Root mean squared error
SST	Sea surface temperature
WFS	West Florida shelf

ABSTRACT

The goal of this study is to quantify the transport mechanisms in the Florida Big Bend Region that contribute to reef fish productivity as a function of the regional physical oceanography. The primary focus of the research is to identify pathways responsible for transporting gag grouper larvae from their offshore spawning grounds to inshore seagrass nurseries. More specifically, the role of variable wind stress and the conservation of potential vorticity are investigated for their role in setting the net across-shelf transport. The primary tool used to address these goals is a very high horizontal resolution (800-900m) numerical ocean model configured for the region and nested within the data-assimilative Gulf of Mexico Hybrid Coordinate Ocean Model. Four contemporaneous simulations using this ocean model are forced with different atmospheric products of varying spatial and temporal resolution. Significant cross-shelf flow is generated during upwelling-favorable wind events, and the mean springtime shelf circulation is set by the rectification of flow during northwesterly or southeasterly-directed wind stress. A Lagrangian particle advection model is used as a proxy for the larval migration, in order to determine the physical pathways for onshore transport. Particle advection experiments indicate that the flow is mostly barotropic and conserves potential vorticity, leading to cross-isobath movement during northwesterly winds. While there is significant interannual variability in the distribution of particles across the shelf, the primary pathway by which particles are able to reach the nearshore environment is presented. The results also indicate that the preferred release locations for particles that successfully arrive inshore coincide with a known gag spawning aggregation site. The results presented in this dissertation provide, for the first time, a description of the mechanisms by which onshore transport is possible from gag spawning sites at the shelf break to seagrass nurseries at the coast.

CHAPTER 1

INTRODUCTION

The Big Bend region (BBR) of Florida in the northeastern Gulf of Mexico (NEGOM) exists at the juncture of the Florida Peninsula and the Florida Panhandle, and where the coastline orientation changes by roughly 90^o. The vast expanses of sea grass meadows along the coastline and the numerous reefs across the BBR provide both nursery habitats and spawning sites for a plethora of marine species. These ecologically diverse and economically productive marine ecosystems of the BBR have been studied for fisheries production (e.g. Hood and Schlieder 1992; Koenig and Coleman 1998; Koenig et al. 2000; Gentner 2009).

Commercial and recreational fishing in the Gulf of Mexico (GOM henceforth, or simply the Gulf) has raised considerable concern in response to reductions in both adult fish abundance and juvenile populations, where recreational fishing accounts for over 60% of annual landings of certain fish species (Coleman et al. 2004). While fishing pressures affect the abundance of adult fish, the density-independent processes that occur during their egg, larval, and early juvenile stages are significant in determining the interannual variability in recruitment (Rothschild 1986; Chambers and Trippel 1997). Thus, understanding recruitment processes of fish species is crucial for their effective management (Fitzhugh et al. 2005).

The physical oceanographic state can largely affect the egg and larval stages of reef fish development by setting their dispersion patterns as well as influencing locations containing available food (Rothschild and Osborn 1988; Werner et al. 1997). With motions of fertilized eggs and many early-stage larvae remaining largely planktonic (Norcross and Shaw 1984), ocean currents may provide most of their horizontal dispersion. Furthermore, the circulation can set the distribution of food sources in the region, which mostly come from the nutrient-

laden, high-chlorophyll coastal waters or via nutrient fluxes from the deep-ocean (He and Weisberg 2003). By moving fish eggs and larvae to or from areas that are conducive for survival, the circulation can directly influence the recruitment and year-class strength of a given species (Norcross and Shaw 1984).

One particular species in the BBR that relies on the circulation for the pelagic stage of its early life cycle is the gag grouper (*Mycteroperca microlepis*; Keener et al. 1988; Fitzhugh et al. 2005; Koenig and Coleman 1998). Indeed, gag is among the most valuable finfish in the region, as it provides over $100 million in value added and over $60 million in income to the economy of the southeastern United States from recreational fishing alone (Gentner 2009). Despite the economic importance of the gag fishery and the gag's presence as a top-level predator, there remains scarce knowledge about the early pre-settlement life stages of this particular fish. Adult gag spawn on offshore reefs along the continental shelf break each spring (February-April; Hood and Schlieder 1992; Coleman et al. 1996), after which their larvae are transported across the shelf until eventually settling as juveniles in sea grass nursery habitats along the coast (Koenig and Coleman 1998). However, the physical mechanisms responsible for this onshore larval transport remain unknown. This emphasizes that a 4-dimensional understanding of the ocean circulation is needed in order to understand the processes affecting larval dispersion in the BBR (Fitzhugh et al. 2005). Understanding these processes *a priori* can eventually aid the management of the gag fishery by improving predictions of the number of successful recruits from year to year.

The material presented in this dissertation fills the need for a 4-dimensional understanding of circulation features and transport mechanisms through the use of high-resolution ocean modeling experiments. The following section provides a review of previous studies, a statement of the remaining open questions, and the specific objectives addressed in this dissertation.

CHAPTER 2

BACKGROUND

The Gulf of Mexico is a semi-enclosed basin connected to the Atlantic Ocean by the Straits of Florida and to the Caribbean Sea via the Yucatan Channel (He and Weisberg 2002a). The GOM features a deep interior (depths $>$ 4km), and continental shelves surrounding nearly the entire basin. The shelves are of variable width and their bathymetries are of varying complexity. In the NEGOM, the continental shelves are particularly noteworthy, where the West Florida shelf (WFS) has one of the widest shelves in the Gulf (150 - 200 km wide) adjacent to the relatively narrow (40km at its narrowest point) Florida Panhandle Shelf (FPS). The transition between these two shelves occurs in the BBR offshore of Cape San Blas (CSB) and Cape St. George (CSG), where the isobaths converge and undergo tight curvature (figure 2.1).

While the BBR has no official boundaries, it is characterized for this study by the notable bend in the Florida coastline ranging from St. Andrew's Bay in the West along the coast to roughly Chassahowitzka Bay in the South. The shelf break features numerous reefs and productive spawning grounds for many warm-temperate reef fish, including the gag grouper (Koenig and Coleman 1998), and the extensive seagrass beds near the coastline provide habitats for many finfish and shellfish populations of significant economic value (Morey et al. 2009). There are several major rivers that drain into the region, namely the Apalachicola, Choctawhatchee, and Suwannee Rivers. The Apalachicola River is by far the largest (annual mean discharge 736 m^3/s; Morey et al. 2009), and perhaps the most influential river in the region, because it is considered to be a key source for the nutrient distribution across the WFS during the late winter and early spring (Gilbes et al. 1996; Morey et al. 2009).

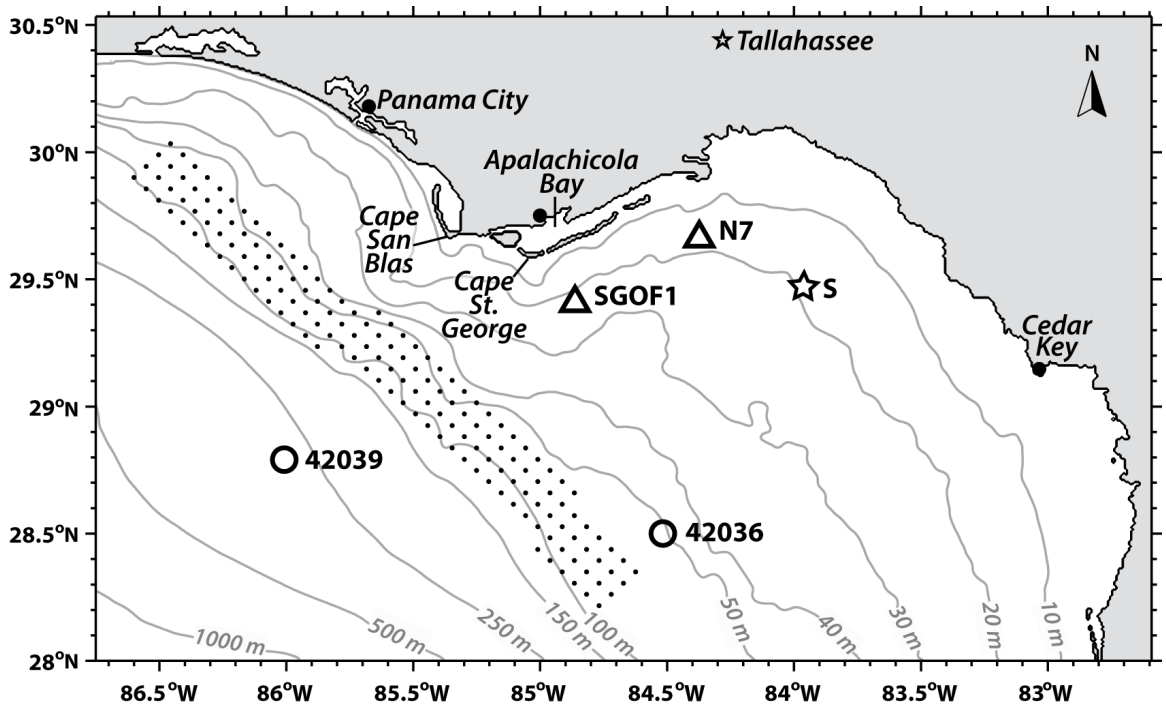

Figure 2.1: The Florida Big Bend Region domain. Grey contours denote the isobaths from the high-resolution ocean model configured for the domain. Triangles depict observational towers, open circles represent NDBC buoys, closed circles represent coastal sea level stations, dots depict Lagrangian particle seeding locations, and the star denotes the location of the current profiler at site S.

While Morey et al. (2009) note that the impacts of the nutrient and freshwater inputs from the Apalachicola River on the marine ecosystems remain unclear, the implications of their study suggest that such high nutrient concentrations (allowing for increased primary production), contribute to increased food availability for ichthyoplankton across the NE-GOM shelf. Due to the direct relationship between food availability and recruitment class size (Cushing 1975, 1990), the nutrient-laden waters of the Apalachicola River are considered to be a large contributor to the regional fishery. Furthermore, since the BBR is one of few regions on the WFS where upwelled deep water interacts with coastal waters, these two sources of high-nutrient waters could enable the Florida Middle Grounds fishery to remain so productive (He and Weisberg 2002b).

The extensive seagrass beds of the BBR can exist in depths up to 20m, and to distances

of up to 50 km offshore (Iverson and Bittaker 1986; Continental Shelf Associates 1997). However, their coverage is not always continuous to those depths and distances offshore, and they can be significantly affected by flood-stage river outflow and tropical storms (Carlson et al. 2010).

2.1 Gag Grouper

The gag grouper (Family *Serrendane*, subfamily *Epinephelinae*) is a common protogynous hermaphrodite. Adult gag spawn as early as January and into April on hard relief bottom or reefs along the shelf break (50-90 m depth; Coleman et al. 1996; Koenig et al. 2000; Fitzhugh et al. 2005), with peak spawning occurring in February and March (Hood and Schlieder 1992). Their larvae spend anywhere from 30-60 days (mean $\sim$ 43 days) in the water column before settlement (a period known as their pelagic larval duration or PLD) in seagrass habitats along the Florida coast some 70-600 km away (Koenig and Coleman 1998; Fitzhugh et al. 2005). At this stage, the gag metamorphose into juveniles and take on a benthic existence (Mullaney and Gale 1996; Koenig and Coleman 1998). The year-class strength of the local fishery is strongly correlated with juvenile abundance in the seagrass habitats near the coast, which can vary 200 fold between high and low settlement years (Fitzhugh et al. 2005). However, while knowledge of spawning characteristics and settlement patterns have been documented in detail (Coleman et al. 1996; Koenig and Coleman 1998; Koenig et al. 2000; Fitzhugh et al. 2005), there remains a large gap in the scientific knowledge of gag larvae during the time of their ingress.

In an attempt to bridge this gap, sampling efforts have been aimed at observing various ichthyoplankton across the NEGOM shelf and other areas where gag are known to spawn (SEAMAP, in coordination with the National Marine Fisheries Service). Although the *Serranidae* are found to be one of the more abundant families taken in collections of ichthyoplankton across the southeastern coast of the US, the GOM, and the Caribbean, the subfamily *Epinephelinae* have not been found to be among those collected (Keener et al. 1988). While gag are prevalent throughout the Gulf and off the Southeastern coast of the US, their spawning characteristics and larval behavioral patterns may vary by region. In fact, Fitzhugh et al. (2005) divided the eastern GOM into three different regions based on

gag spawning and settlement times. One these regions designated by Fitzhugh et al. (2005) is the NEGOM, north of 28^{o}N and east of St. Andrew's Bay.

Keener et al. (1988) assessed the ingress of postlarval (pre-settlement, but without juvenile pigmentation) gag through a South Carolina barrier island inlet, discovering a relationship between lunar cycle, local tides, and ingress of gag. They find that the majority of postlarvae arrived inshore in the upper 3m of the water column at night, particularly in association with the flood tide. The work by Keener et al. (1988) suggests that gag either exhibit a diel vertical migration in order to remain in preferred estuarine locations, or simply settle immediately along the bottom in order to prevent seaward transport during the ebb tide. That being said, Keener et al. (1988) do not assess those factors which transport larvae from the offshore spawning locations to the nearshore inlets where postlarval gag were captured. These transport processes on the shelf could likely be very different from the nearshore environment. This is particularly true in the NEGOM, where residual tidal currents are much weaker than at the same latitude in the Atlantic (He and Weisberg 2002a; Zetler and Hansen 1971).

One of the only works to estimate the transport mechanisms of postlarval gag in the NEGOM is that by Fitzhugh et al. (2005). Their study uses information from juveniles collected in trawls through seagrass beds of the BBR (and also for a region south of 28^{o}N) in order to calculate temporal variations of spawning, fertilization, settlement, and PLD. In addition, they constructed an empirical model of near-surface ocean currents from buoy observations to estimate horizontal near-surface transport. However, since there is no known knowledge of the vertical migratory behavior of gag larvae, they only assessed the transport of larvae that would remain at the surface. Their conclusions revealed that near-surface currents driven by wind forcing alone could not provide the necessary mechanism for onshore transport anywhere along the WFS. They recommend the use of a fully three-dimensional physical model to properly assess the role of currents in all directions and at all depths.

2.2 Circulation in the NEGOM

The general circulation in the interior of the GOM is largely driven by the intrusion of the western boundary current that enters through the Yucatan Channel, forming the famous

Loop Current (LC; Morey et al. 2005). The LC is the dominant energetic current in the interior GOM, and its influence on the circulation near the shelf break has been clearly documented (Weisberg et al. 1996; Meyers et al. 2001; He and Weisberg 2003; Barth et al. 2008). He and Weisberg (2003) illustrate, through observations and some idealized model experiments, that currents along the WFS break are dominantly controlled by intrusions of the LC upon the WFS. They further suggest that the influence of these intrusions are generally constricted to within one radius of deformation ($R_d \sim 35$ km), nearly 4-5 times narrower than the width of the WFS.

The ocean's circulation on continental shelves is driven by a combination of local surface forcing, rivers, tides, and deep-ocean fluxes near the shelf break (Morey et al. 2005; Weisberg et al. 2005). However, the most dominant forcing mechanism on the WFS and FPS is the wind-driven component of this forcing, as the NEGOM shelf circulation has a strong relationship with the local wind stress (Mitchum and Clarke 1986; Morey and O'Brien 2002; Morey et al. 2005; Weisberg et al. 2005).

From late fall through most of the spring, the winds are dominated by synoptic-scale weather systems (cold fronts; Clarke and Brink 1985). Pre-frontal winds typically range from the south to the east, and upon the passage of cold fronts, these winds will rotate relatively quickly (on the order of 10 minutes to hours) to a westerly to northerly origin. For the BBR, winds with a southeasterly component are downwelling-favorable, whereas winds with a northwesterly component are upwelling-favorable, via the surface Ekman transport. During the summer months, the development of sea-breeze system provides the dominant variability of winds near the coast. However, as the sea-breeze system typically does not fully develop until the summer, it's contribution to cross-shelf transport during the springtime is not discussed here. The strength, duration, and frequency of upwelling-favorable winds varies highly on interannual timescales. Weisberg and He (2003) illustrated that varying only the local mean monthly wind stress in a model of the NEGOM for two separate years varied the shelf circulation patterns and the amount of upwelling considerably. In fact, they attributed most differences in circulation patterns and upwelled water properties on the shelf between the two years to the difference in the strength and duration of upwelling-favorable wind events.

The transition from wintertime synoptic-scale dominance to the more quiescent summertime wind patterns, along with a changing surface heat flux from net cooling to net warming, manifests itself through changes in the ocean circulation. Indeed, the spring is a period when typical wintertime horizontal stratification on the shelf gives way to vertical stratification, as surface heating induces thermocline development (Morey and O'Brien 2002; He and Weisberg 2002b). Consequently, this spring transitionary period features a mid-shelf southeastward current, cold and low salinity tongues, and a high chlorophyll plume (He and Weisberg 2002b). He and Weisberg (2002b) find that the wind stress drives a circulation that is strongest near-shore in the BBR, while a cyclonic heat flux-induced baroclinic circulation adds constructively (destructively) to the mid-shelf (near-shore) wind-driven circulation. They suggest that the interplay between the local momentum and buoyancy forcing creates a mid-shelf jet that flows southeastward along the WFS (He and Weisberg 2002b). As surface heating persists throughout the spring, the baroclinic circulation recedes, a bifurcation of the coastal current near Cape San Blas disappears, and the jet strengthens and moves slightly offshore (He and Weisberg 2002b).

The baroclinic circulation in the BBR has impacts beyond strengthening or relaxing the Big Bend Gyre. With the existence of upwelling and net surface cooling of coastal water during the winter months, the combined springtime relaxation of negative surface heat flux and increased river streamflow add to create a cold tongue that extends south along the mid-shelf (He and Weisberg 2002b). This cold tongue is a major contributor to the cyclonic circulation in the BBR. In fact, using modeled Lagrangian drifters, He and Weisberg (2002b) find that the changes in hydrography during the spring transition help promote onshore transport near the bottom from the shelf break to mid-shelf in the BBR.

The presence of a riverine-induced salinity front near the coast can allow shoreward flows to develop in the bottom layer and more complex flows near the interface of the front (Weatherly and Thistle 1997; Lentz 2012). Under light winds, the buoyant current formed by the Apalachicola River will tend to the right, flowing westward around the horn of CSB (Morey et al. 2009). However, as Morey et al. (2009) note, strong winds associated with the passage of atmospheric cold fronts force this low-salinity (and high chlorophyll) water offshore. This phenomenon, described as the 'Green River,' only occurs after strong

forcing in conjunction with these frontal passages (Gilbes et al. 1996; He and Weisberg 2002b; Morey et al. 2009). The coastal waters, in conjunction with local surface cooling, can produce areas of low temperature and salinity and high nutrient content on the inner shelf. Then, mixing with upwelled deep ocean water on the shelf produces the cool and low salinity tongues that can persist over the mid-shelf well into the summer months (He and Weisberg 2002b; Weisberg and He 2003).

Tides in the Gulf of Mexico are relatively small in comparison with tidal amplitudes from other locations around the world at similar latitudes. The largest tidal constituents in the GOM are the diurnal tidal constituents (K_1 and O_1; He and Weisberg 2002a). This is in stark contrast to the Atlantic Coast at the same latitude, where the semidiurnal tide dominates (He and Weisberg 2002a; Zetler and Hansen 1971). The largest tides occur along the WFS and in the BBR, with the barotropic component remaining relatively small (He and Weisberg 2002a; Gouillon et al. 2010). Tidal velocities rarely exceed a few cm/s, and particle displacements from the barotropic tidal current remain on the order of 10 km per month (He and Weisberg 2002a). Thus, while Keener et al. (1988) showed a relationship between tides and gag larval transport in South Carolina, their relatively small impact on the overall transport of materials on the NEGOM shelf excludes tides from being of primary interest for this study.

The observational record in the BBR remains sparse, with most observational efforts focused offshore of Tampa Bay on the WFS, or to the west near Louisiana (e.g. Niiler 1976; Mitchum and Sturges 1982; Mitchum and Clarke 1986; Weisberg et al. 1996; Meyers et al. 2001; He and Weisberg 2002b). The more permanent observational networks remain to the west of Tampa Bay, south of the region of immediate interest for this dissertation. However, results from these observational programs provide useful insight into dynamics affecting the WFS circulation. For example, the influence of the LC on shelf break currents, and the inshore extent to which the LC exerts its influence have been described by several different works (Barth et al. 2008; Meyers et al. 2001; Weisberg et al. 1996). Also, much of the observational work has provided evidence that the WFS circulation and sea level variations are highly correlated with variations in the synoptic scale wind stress (Mitchum and Clarke 1986; He and Weisberg 2002b; Maksimova 2012). These observations are generally limited

to ADCP records, coastal tide gauge data, and a few transects across the WFS.

Several surface drifter experiments have taken place in the NEGOM, from the drifter bottle experiments in the 1960s and 1970s (Tolbert and Salsman 1964; Gaul 1967; Williams et al. 1977), to the extensive SCULP project run by the Mineral Management Service (MMS; Yang et al. 1999; Sturges et al. 2001; Ohlmann and Niiler 2005). The major finding of these results, particularly those from the SCULP project, is that virtually no drifters have ever arrived inshore along Florida's west coast, south of Apalachicola. This led for this region with no drifter tracks to be aptly named "The Forbidden Zone" by Yang et al. (1999), and suggests that onshore transport likely occurs in layers other than the surface. In fact, Yang et al. (1999) suggest that onshore transport in the southern portion of the BBR occurs in the bottom layer, due to a slight convergence of isobaths in this region. While these works provide useful analysis of observations along the NEGOM shelf, a large gap remains in observations across the BBR, and questions regarding cross-shelf transport have yet to be fully addressed.

The overall lack of observations in the BBR has been somewhat bridged by numerous modeling studies of the region (e.g. Weisberg et al. 2001; He and Weisberg 2002b, 2003; Morey et al. 2005, 2009; Barth et al. 2007, 2008). A series of studies (e.g. He and Weisberg 2002a,b, 2003; Weisberg et al. 2001) used a model configured for the eastern GOM to investigate different process studies on the WFS. These studies mainly focused on the general circulation across the NEGOM shelf, from Mississippi to the Florida Keys. In particular, they assessed the role of wind forcing, surface heat fluxes, and tides on the general circulation of the NEGOM. In the process, He and Weisberg (2003, 2002b) also discussed the transitionary periods of Fall 1998 and Spring 1999, respectively. All of these previous modeling studies provide a great foundation for the work to be presented in the following sections, as they describe many of the relevant circulation features and the contribution of varying forcing mechanisms to the formation of those features.

With the exception of the works by Morey et al. (2005, 2009), the only discussions of cross-shelf transport in the BBR from the aforementioned modeling studies remain speculative. In fact, even Morey et al. (2009) were concerned only with the relationship between the cross-shelf transport of low-salinity waters and ocean color imagery in order to further

the understanding of the 'Green River' generation mechanisms. While their study implies several different consequences of this low-salinity / high chlorophyll content in regards to the regional fishery, the mechanisms for transport of materials from the shelf break to the coast remain largely undiscussed in previous works. One attempt to understand the physical transport mechanisms of gag larvae in the BBR is that by Fitzhugh et al. (2005). They find that, although surface transport is generally directed northward along the WFS, the surface layer transport by wind alone does not produce the necessary cross-shelf transport for gag larvae, and concede that a fully three-dimensional approach at understanding these processes is needed.

2.3 Research Overview

This review of previous studies indicates that a detailed knowledge of the physical transport processes in the BBR is needed in order to understand the early stages of the gag grouper's life cycle. While the timing and locations of gag spawning aggregations have been described (i.e. Coleman et al. 1996; Fitzhugh et al. 2005), there remains a gap in the previous studies about the processes affecting gag grouper during their time of ingress to the seagrass nurseries (Fitzhugh et al. 2005). It is understood that the shelf circulation during the spring months is set largely by the local wind stress, although it is unclear how the circulation in the BBR evolves in 3-dimensions and how it responds to higher frequency variations in the wind stress. Finally, it remains to be determined how the circulation features in the region contribute to the onshore transport of gag larvae during the spring. This dissertation aims to fill a portion of this gag in knowledge by assessing the impact of the physical transport on setting the distribution of materials across the shelf. In particular, this study focuses on three outstanding research questions:

1. What is the influence of variable atmospheric wind stress on the major circulation features of the Florida Big Bend shelf?

2. What are the physical mechanisms by which cross-shelf transport is possible during the spring months?

3. Are the physical transport mechanisms in the BBR capable of providing the necessary transport for gag larvae from the shelf break to coastal seagrass nurseries?

The results of this study are expected to provide a basic foundation for fisheries ecologists to understand the potential pathways by which gag larvae are able to arrive in their nursery habitats each spring. This will enable further interdisciplinary research into the physical characteristics and ecology of the region and will unlock a portion of the mystery that surrounds the early part of this particular reef fish's life cycle. Also, since this study focuses on the physical transport mechanisms in the region, the results are also expected to be applicable to the transport of a variety of environmentally-important materials (i.e. pollutants, oil spills, harmful algal blooms, etc.) into the BBR. In chapter 3, the impact of wind stress variability on the major shelf circulation features are discussed using four contemporaneous ocean model simulations. Then, in chapter 4, the mechanisms are determined for which cross-shore transport is possible. The pathways by which these mechanisms allow for the necessary transport of gag larvae is also discussed. Finally, conclusions and the future of this work is discussed in chapter 5.

CHAPTER 3

THE IMPACT OF VARIABLE ATMOSPHERIC FORCING ON THE SPRINGTIME CIRCULATION IN THE BIG BEND REGION

The BBR is a historically under-studied area of the world's ocean, yet this region's marine ecosystems remain a viable economic source for the southeastern United States. Valuable fish species in the region rely on the regional circulation for survival during the early stages of their life cycle. The findings from previous studies in the region outlined in chapter 2 indicate that the primary driver of the shelf circulation on the WFS and BBR is the flux of momentum from the atmosphere. Thus, the aim of this chapter is to describe the variability of the wind stress over the region, and to demonstrate how varying representations of the atmospheric state affect the ocean circulation in the BBR. Finally, this chapter describes the dominant flow features during the springtime, and their variability on multiple scales. This is done by analyzing various atmospheric products and through several contemporaneous ocean model simulations.

3.1 Introduction

The Florida BBR is an area that has lacked significant focus in previous studies of shelf circulation processes in the GOM. Section 2.2 indicates that most studies have either been relatively short-lived or have been concerned with flow features further to the south or west, where major ports are located. However, the short-lived observational studies (e.g. Marmorino 1983; Mitchum and Clarke 1986; Weatherly and Thistle 1997) in the region have all indicated that there exists a strong relationship between the local wind stress and

the shelf circulation, a finding that is emphasized over broader spatial scales in several modeling studies whose domains include the BBR (e.g. Li and Weisberg 1999a,b; Morey et al. 2005; Weisberg et al. 2005). The observational studies mostly focus on the ocean's response to large-scale, low frequency wind forcing, and not the response to winds that have higher spatial or temporal variability. This large-scale, low frequency variability during the springtime is provided by the passage of cold fronts, which have phases of downwelling (pre-fontal passage) and upwelling (post-frontal passage) favorable wind stress over the WFS and BBR. The strength and frequency of upwelling favorable events may vary on multiple time scales, and the response of the shelf circulation can be quite different based on the direction of the winds (Li and Weisberg 1999a,b).

While the dominant variability in the springtime occurs at synoptic scales, it is unclear from the previous literature what impact a higher degree of spatial and temporal variability in the winds may have on the shelf circulation. Weisberg et al. (2005) discuss the variability of the WFS circulation on multiple time scales (from synoptic scales to interannual fluctuations). They find that the while the synoptic weather systems dominant the circulation features within each season, there are significant variations between seasons and between years. The interannual fluctuations in the strength and frequency of frontal passages could be affected by large-scale changes in weather patterns, such as those associated with the phase of el Niño / Southern Oscillation (ENSO). The positive (negative) correlation between ENSO phase and precipitation (500 hPa heights) over the southeast suggests that years with a positive ENSO phase (el Niño) years may expect stormier weather (i.e. more frontal passages; Hoerling and Kumar 2001; Ropelewski and Halpert 1986). Therefore, el Niño years may expect more frequent, and potentially stronger, frontal passages. For the remainder of this dissertation, the spring is defined as February through May, as this period of time covers most of the spawning and PLD for gag grouper in the BBR.

It remains to be addressed how higher temporal or smaller spatial-scale variations in the wind stress affect the response of the coastal ocean circulation during the spring months. In particular, the response of the shelf waters in the geometrically intriguing BBR remain to be fully discussed from a fully 4-dimensional approach. Therefore, this chapter is focused on the impact of a varying atmospheric state on the major features of the springtime BBR shelf

circulation. In the following sections, a description of the variability of springtime winds over the BBR is given using various atmospheric products as varying atmospheric representations. These products are used as surface forcing for four contemporaneous ocean model simulations. Next, a comparison of model results to a variety of observational platforms in the region is given. A description of the mean circulation features and the variability in the flow on multiple time scales then follows.

3.2 Wind Variability

One aim of this chapter is to understand how variations in the dominant forcing mechanism over the BBR affect the major features of the shelf circulation. Therefore, varying manifestations of the atmospheric state are provided via output from four different atmospheric models of varying spatial and temporal resolution. Two of these datasets are reanalysis products developed and operated by the National Center of Environmental Prediction's (NCEP) Environmental Modeling Center, while the other two datasets are data-assimilative hindcast / nowcast model runs developed and operated by the United States Naval Research Laboratory (NRL). Therefore, all four products are state-of-the-art prediction systems that are bound to observations through advanced assimilation schemes. In addition to varying model physics and assimilation methods, each product provides a different combination of horizontal grid spacing and temporal resolution (see table 3.1), allowing the impact of varying resolution on the resulting ocean circulation features to be assessed. The four different datasets will be discussed, along with the variability among and between them. Comparisons are made to regional meteorological observations from buoys to assess the accuracy of each product with respect to observations. The atmospheric datasets are then used to force a regional ocean circulation model.

3.2.1 Description of the datasets

The two reanalysis products used in this study are the Climate Forecast System Reanalysis (CFSR) and the North American Regional Reanalysis (NARR). The CFSR is a global coupled ocean-atmosphere-land-sea ice modeling system that uses the NCEP Global Data Assimilation System (GDAS), and is described in great detail in Saha and Coauthors

(2006). It is the newest product of the four chosen models, which is notable in that it incorporates more data into its assimilation system (notably scatterometer winds and direct assimilation of satellite-derived radiances). This product also provides the highest temporal resolution (hourly) of the four atmospheric datasets. The hourly output fields are provided in the form of analysis fields every 6 hours, with hourly forecast fields for the intermediate time steps. The NARR is an atmosphere-land hydrology coupled model, which is run for regional application to North America (for more details see Mesinger and Coauthors 2006) at roughly $1/3^o$ horizontal grid spacing and available at an output frequency of 3 hours. NARR is based on the NCEP Eta atmospheric model, and uses its associated 3D variational technique for assimilation of observations (Mesinger and Coauthors 2006).

The Navy Operational Global Atmospheric Prediction System (NOGAPS) and the Coupled Ocean/Atmosphere Mesoscale Prediction System (COAMPS) are operational, data-assimilative models available from the NRL (see Hogan and Rosmond 1991; Rosmond 1992; Hodur 1996). The NRL's Central America COAMPS configuration is used in this study. It is run as an uncoupled atmospheric model using the Navy's multivariate optimally interpolated (MVOI) data assimilation system (Goerss and Phoebus 1992; Barker 1992) and provides the highest horizontal grid spacing for this study, at 0.2^o. NOGAPS, which also uses the MVOI data assimilation system, has the coarsest grid spacing for this study at 0.5^o, with 3-hourly output. The NOGAPS is also used to force the $1/25^o$ GODAE Gulf of Mexico HYbrid Coordinate Ocean Model (GOM HYCOM; Bleck 2002; Chassignet et al. 2007, 2009; Chassignet 2011). As will be described in detail in section 3.3, the GOM HYCOM is used to set the open boundary conditions for an ocean model for the BBR. This makes the inclusion of NOGAPS of interest to this study in order use a consistent atmospheric forcing across the model's open boundaries.

3.2.2 Discussion of the variability

The winds from each atmospheric product are compared to observations from three marine observation platforms in the NEGOM (National Data Buoy Center [NDBC] buoys 42036 and 42039, and SGOF1) over the period 2004-2010. Winds are adjusted to a common 10m above the surface using standard height adjustment procedures outlined by Liu and

Model	Grid Spacing	Temporal Resolution	Range
CFSR	T382	1 hour	1979-2009
NARR	$\sim$ 32.46 km	3 hour	1979 - Present
NOGAPS	0.5^o x 0.5^o	3 hour	2003 - Present
COAMPS	0.2^o x 0.2^o	3 hour	2003 - Present

Table 3.1: Atmospheric model grid specifications.

Tang (1996). Unless otherwise mentioned, winds have been low-pass filtered using a cosine-Lanczos filter (Emery and Thompson 2001) to remove variability at frequencies shorter than 30 hours (resulting in sub-inertial or low frequency variability; see Appendix B for more detail on the filtering procedure).

A list of the correlation coefficients and parameter estimates from a linear regression fit between modeled winds and observed winds over the entire 7-year period of 2004-2010 is given in table 3.2.2. Regression slopes that are close to unity indicate that NOGAPS and COAMPS estimate the strength of the observed winds well at sites 42039 and SGOF1, where the models only overestimate wind speeds in the low-wind environment by about 0.4-0.6 ms^{-1}. NOGAPS and COAMPS under-estimate wind speed in the high-wind environment by up to 1 ms^{-1} at these locations. NOGAPS does particularly poor among the products at capturing the variability in wind stress at 42036 ($R^2 = 0.551$), however increased R^2 values at 42039 and SGOF1 indicate that it captures the variability of observed winds much better at these locations. COAMPS captures the variability at all observation locations well, with R^2 values above 0.82.

CFSR estimates the strength of the winds well in the mid to high wind strength environment (slopes close to 1), but under-estimates stronger winds near 42036 by about 1 ms^{-1}. The variability of the winds is captured well by the CFSR at SGOF1 and 42036, where R^2 values exceed 0.95, and the regression line at SGOF1 falls very close to unity (0.9939). Small regression slopes with intercepts near zero indicate that NARR has a systematic weak bias across the NEGOM, particularly in the high wind environment. Despite this weak bias, it captures the variability in the winds at every location well, with all R^2 values remaining above 0.9.

It has been demonstrated throughout the previous studies of the region that the wind

Atmospheric Forcing	Location	Slope	Intercept	R^2
CFSR	42036	0.7706	0.5225	0.9016
	42039	0.9521	0.1760	0.9291
	SGOF1	0.9939	0.0503	0.9312
NARR	42036	0.7062	-0.0038	0.8067
	42039	0.7773	0.1873	0.8120
	SGOF1	0.8154	0.0381	0.8443
NOGAPS	42036	1.045	-0.071	0.820
	42039	0.983	0.441	0.793
	SGOF1	0.9222	-0.844	0.551
COAMPS	42036	0.7462	0.7335	0.8244
	42039	0.8979	0.5071	0.8764
	SGOF1	0.9234	0.3516	0.8732

Table 3.2: Linear regression fits for winds calculated from each atmospheric dataset nearest buoys 42036 and 42039, and Tower SGOF1 observed winds at each location

stress is the dominant forcing mechanism of the shelf circulation. It is useful to assess the strength and frequency of the alongshore component of the wind stress, as this component of forcing correlates well with the dominant shelf flow features (Mitchum and Clarke 1986; Maksimova 2012). In order to compare the dominant frequencies and the strengths of winds acting over the BBR from each atmospheric product, the modeled wind stress is extracted from a mid-shelf point near buoy 42036 and rotated to 30 degrees west of north. This roughly follows the orientation of the continental shelf break across the NEGOM and much of the WFS. The wind stresses, extracted from the contemporaneous ocean model runs described in the the following section, are low-pass filtered using a 2-day running mean, and the power spectra for each model run are calculated for February - May of each year (figure 3.1 shows the spectra within the synoptic band [3-10 days]). A consistent peak in power spectra is observed around 3-4 days each year, with a second and larger peak appearing around 5 days in 2004 and 2005. There is not a well-defined peak within this band for 2008 and 2009, so one may consider the point where the power begins to plateau as the significant signal in these cases (near 3.5 days). Indeed, high-pass filtering the data elucidates this particular peak in the power spectra. The mean and standard deviations in the period of these local maxima are 4.386 days and 0.747 days, respectively. The reduced power for NARR wind stress in figure 3.1 highlights the previously discussed weak bias in

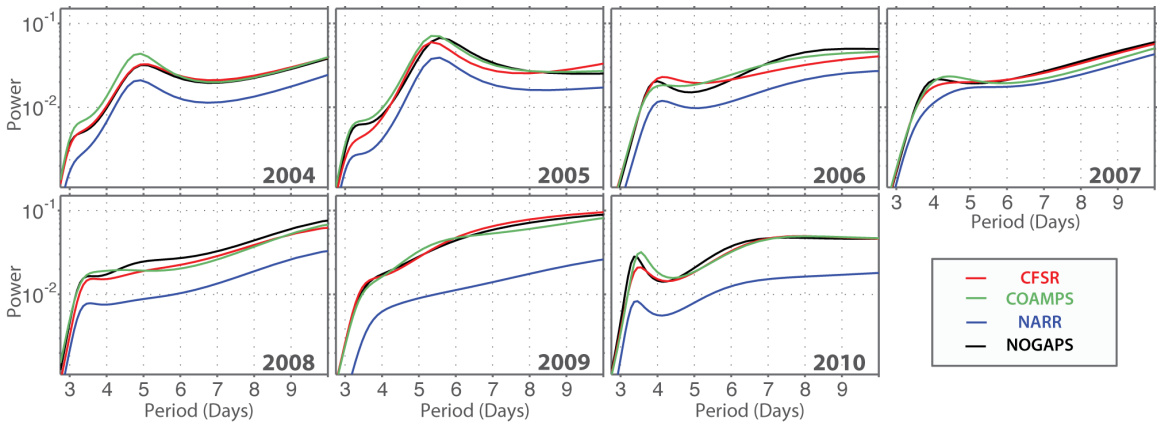

Figure 3.1: Synoptic band of the alongshore wind stress power spectra during the spring months, calculated using the maximum entropy method.

this atmospheric product's winds.

The wind during the spring months has downwelling-favorable and upwelling-favorable phases. Figure 3.2a demonstrates that over the 7-year period, the springtime winds are dominantly of easterly origin. The lengths of the bars in figure 3.2a demonstrate that while winds from the northwest are less frequent than easterly winds, they are also stronger. This can also be seen in figure 3.2b, as the distribution of winds from the northwest is shifted towards stronger winds. Finally, figure 3.2 indicates that winds originating from the southwest are not only much less frequent during the spring months, but also much weaker. This is consistent with the idea that the wind stress' dominant frequency of variability occurs with the passage of cold fronts, where pre-frontal winds range from the east-southeast and quickly rotate to the northwesterly quadrant before gradually turning clockwise to the east again.

The springtime winds over the BBR have been analyzed using four different atmospheric products. The inter-product comparison demonstrates that all products capture the dominant frequency in wind stress spectra, but vary in the strength and exact timing of the changes in wind stress. Each product is now used to force an ocean model, which provides for an assessment of how varying atmospheric representations affect the shelf circulation in the BBR.

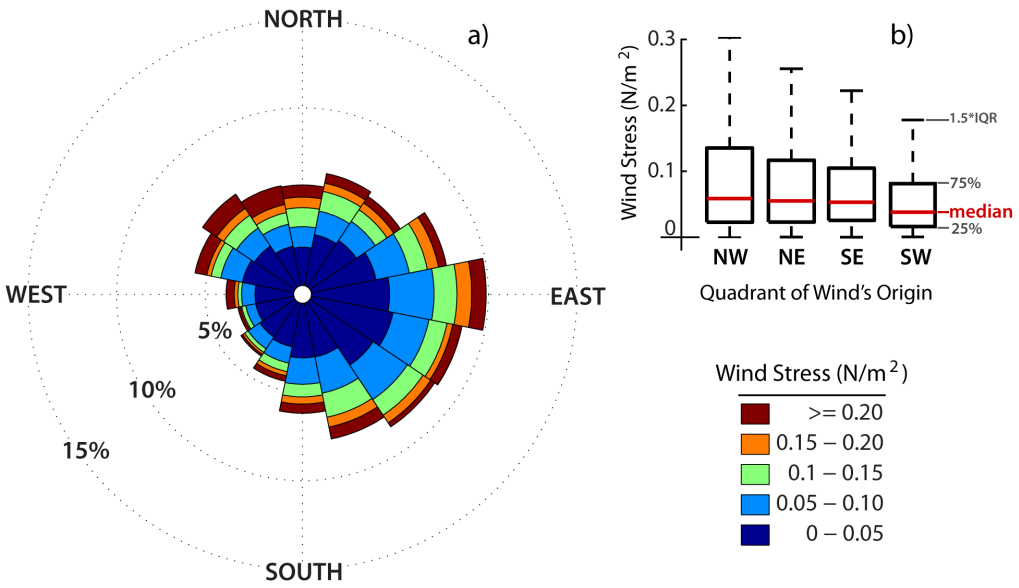

Figure 3.2: a)Wind stress rose for 7 years of springtime wind stresses taken from the ocean model simulation forced with CFSR, and b) box and whisker plots demonstrating the distribution of springtime wind stress originating from each direction. Vertical box edges indicate the upper and lower quantiles, and hash marks designate 1.5 times the interquartile range (IQR). Red lines indicate the median value. Direction of boxes on the wind rose indicate the direction from which the wind stress originates.

3.3 Description of the ocean model

The Regional Ocean Modeling System (ROMS; Shchepetkin and McWilliams 2003, 2005) is the ocean modeling system that is chosen for the BBR. ROMS is a free-surface, terrain-following, primitive equation ocean model that is frequently used for shelf and coastal applications (Shchepetkin and McWilliams 2005). The vertical s-coordinate of ROMS provides a constant number of terrain-following layers that effectively increases the vertical resolution of the model over shallower depths. While it has been shown that non-alignment of the vertical coordinate isosurfaces to isopycnals or geopotential surfaces in terrain-following coordinate models can lead to erroneous mixing in association with the calculation of the horizontal pressure gradient (Marchesiello et al. 2009; Lemarié et al. 2011), advanced advection schemes and the choice of domain are capable of limiting the errors associated with these calculations. With the advanced numerical schemes and modules provided by ROMS,

it is able to be adapted for a variety of applications, and as such it is chosen as the modeling system to be configured for the BBR.

The choice of modeling domain is dependent on factors that can affect the circulation in the BBR. That is, one must choose the model domain and grid spacing to not only resolve the relevant small-scale processes in the BBR, but also to properly capture the larger-scale features that influence the general circulation in the region. Thus, the BBR configuration of ROMS (henceforth BBROMS) is configured on a rectangular-shaped domain with a uniform $1/120^o$ grid spacing that extends north of 28^oN and east of 86.75^oW to the Florida coastline (see figure 2.1). This horizontal grid spacing is fine enough to resolve buoyant coastal river plumes while still remaining computationally efficient. The choice of domain allows the shelf to be covered beyond the inner shelf break (∼70-100m depth), while also capturing the northern zoogeographic region defined by Fitzhugh et al. (2005). In addition, this choice of domain allows for model comparison with several different observational platforms. This includes the three NDBC observational platforms, 5 years of nearly continuous measurements from a bottom-mounted Acoustic Doppler Current Profiler (ADCP) at site N7, an additional bottom-mounted current profiler deployed for just over one year at site S, and three coastal tide gauge stations (figure 2.1). The contemporaneous ocean model simulations are initialized on 01 Jan 2004 and run continuously through 31 Dec 2010.

The model's initial conditions and temporally-evolving open boundary conditions are provided by the GOM HYCOM. The GOM configuration of HYCOM has $1/25^o$ horizontal grid spacing at the equator, a latitudinal grid spacing of $(1/25)^o \times \cos(\text{lat}) \sim 3.5$ km for each variable at mid-latitudes, and 20 coordinate surfaces in the vertical. HYCOM uses the Navy Coupled Ocean Data Assimilation (NCODA; Cummings 2005) system, which assimilates available satellite altimeter observations, satellite and in situ SSTs, as well as available in situ vertical temperature and salinity profiles from XBTs, ARGO floats, and moored buoys. This yields a robust estimate of the ocean state (Chassignet et al. 2009). One attribute of the data assimilative HYCOM system is its capability to provide boundary conditions to higher-resolution regional and coastal models (Chassignet et al. 2009). Indeed, this has been proven to be beneficial for ROMS configurations in the GOM by providing estimates of the major circulation features that are more accurate than models forced by climatology at

open boundaries (Barth et al. 2008). Therefore, the HYCOM's state-of-the-art prediction system provides a robust estimate of the ocean that is well-resolved in space and time, and is thus chosen to provide the best available boundary conditions for the BBROMS. The details of how the model's open boundary conditions are configured, along with a full description of the model specifics, numerical schemes, and forcing specifications may be found in Appendix A.

3.4 Model Validation

The four contemporaneous ocean model simulations are compared to a suite of regional observations to assess their ability in reproducing the observed hydrodynamic and thermodynamic features at each individual location. Observations in the region to which the models are compared include three coastal sea level stations at Cedar Key, Apalachicola, and Panama City, surface temperatures from buoys 42036 and 42039, tower SGOF1, and satellite-derived temperatures provided by the multi-sensor improved sea surface temperature (MISST) 9km blended product (Gentemann and Coauthors 2009). Additionally, the modeled velocities are compared to two bottom-mounted current profiler time series at site N7 and site S. Unless specifically stated otherwise, the previously-mentioned cosine-Lanczos filter is used to compare the sub-inertial flow features. Before filtering the sea level data and observed currents, lunar and solar fortnightly tides have been removed using a least-squared fit (see Appendix B for more information).

3.4.1 Sea level

The simulated sub-inertial sea level is compared to three coastal tide gauge stations operated by the NOAA Center for Operational Oceanographic Products and Services. Each BBROMS simulation reproduces the coastal sea level data well, with correlations over the entire 7-year period greater than 0.8 and with lags around 2hrs, 6hrs, and 3hrs at Cedar Key, Apalachicola, and Panama City, respectively (figure 3.3). Correlations are reduced in the summer months, when the flow varies at much higher frequencies and is generally much weaker in magnitude. This is especially true during the quiescent summer of 2006. Correlations during the spring months are greater than 0.85 for Panama City and Apalachicola

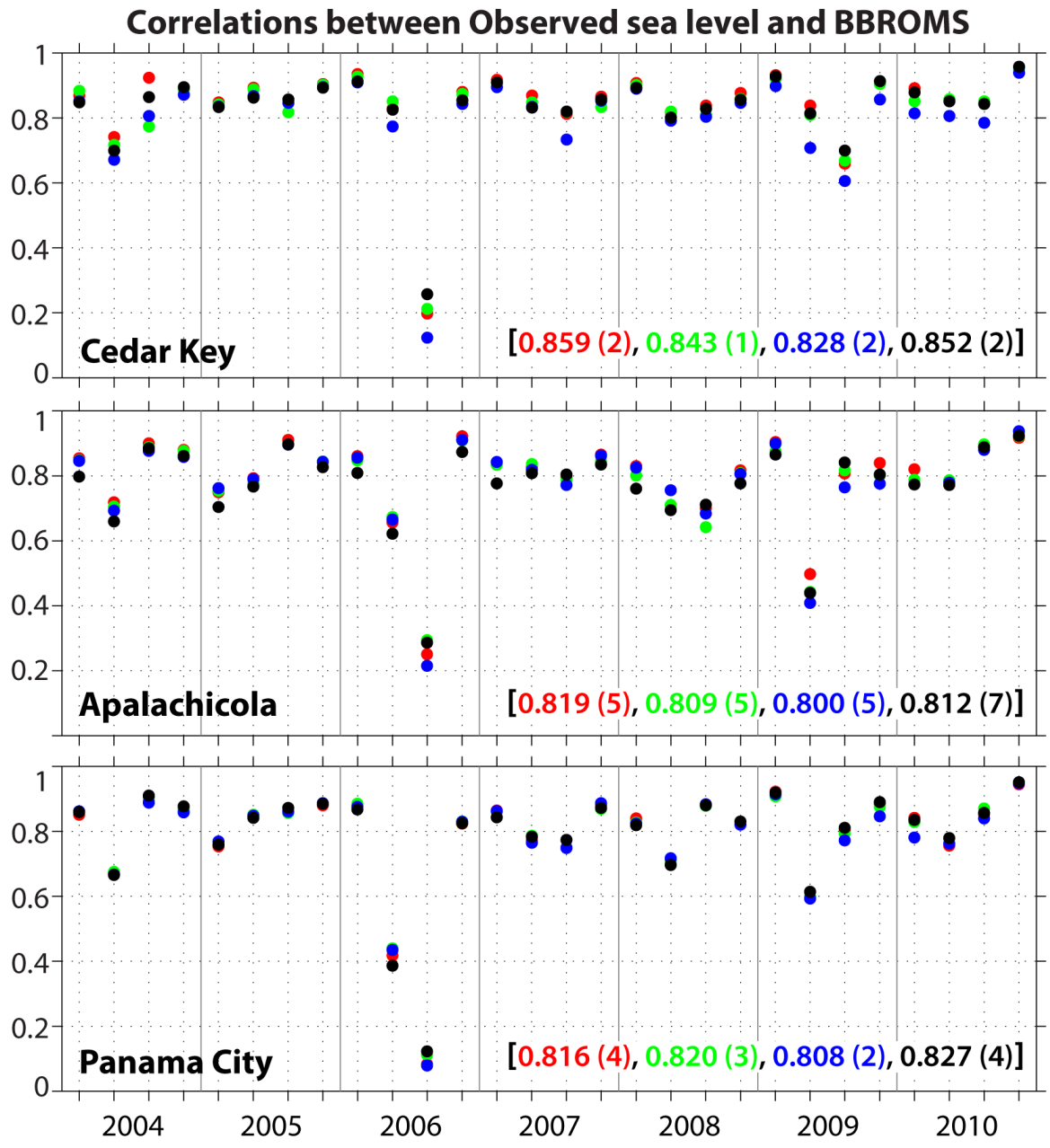

Figure 3.3: Correlations, R, of modeled sea level to observed sea level at Cedar Key, Apalachicola, and Panama City during each quarter (Jan-Mar; Apr-Jun; Jul-Sep; Oct-Dec). Red, green, blue, and black dots depict the correlation during each quarter for BBROMS models forced by CFSR, COAMPS, NARR, and NOGAPS, respectively. The colored numbers represent the maximum lagged correlations calculated for the entire 7-year time series, where numbers in parentheses show the number of hours lag at which the highest correlation is found.

(figures 3.4 and 3.5), and greater than 0.65 for Cedar Key (figure 3.6). The springtime root mean squared error (rmse) falls below 8.5 cm for all model simulations, with the exception of the strong el Niño winter and spring of 2010, when each contemporaneous model simulation has a low sea level bias with an increased rmse of about 11 cm. However, the variability remains highly correlated with the observed sea levels for this year, when correlation values remain greater than 0.8, 0.7, and 0.74 for Panama City, Apalachicola, and Cedar Key, respectively. Indeed, the rmse during spring months remains below 8.5 cm for all other years and model simulations.

3.4.2 Temperature

All models produce surface temperatures that closely match the mean trends observed from the 9km MISST. The variability in the annual mean spatially-averaged SSTs follow the same pattern as those observed from MISST, with CFSR- and NARR-forced models fitting well within the error bounds of the observed values (figure 3.7). BBROMS simulations forced by NOGAPS and COAMPS show a systematic bias toward colder annual mean SSTs when compared to the MISST. The cold bias is due to colder mean SSTs in these two model runs during fall and winter months. In fact, these two simulations closely match the satellite-observed SSTs during the spring and summer, while CFSR- and NARR-forced BBROMS SSTs closely match MISST for all seasons except summer, where they overestimate the temperatures. However, it should be taken into account that the greatest cooling (warming) in the winter (summer) occurs near the coast (more than 2^oC difference in some months), where satellite retrievals are particularly poor due to land contamination. Therefore, the the ability of each model to reproduce the mean SSTs within 0.5^oC should be considered in conjunction with the comparison of each model to observed temperatures at regional buoys.

Modeled SSTs compare well to observed surface temperatures at the three NDBC observational platforms in the BBR. Without any filtering procedures of modeled or observed surface temperatures, R^2 values exceed 0.93 and linear regression fits fall very close to the unity line for all simulations (see table 3.4.2). The agreement between modeled and observed surface temperatures at buoy locations is encouraging, as it demonstrates the ability of each model to capture the sub-mesoscale variability of temperatures at different points across the

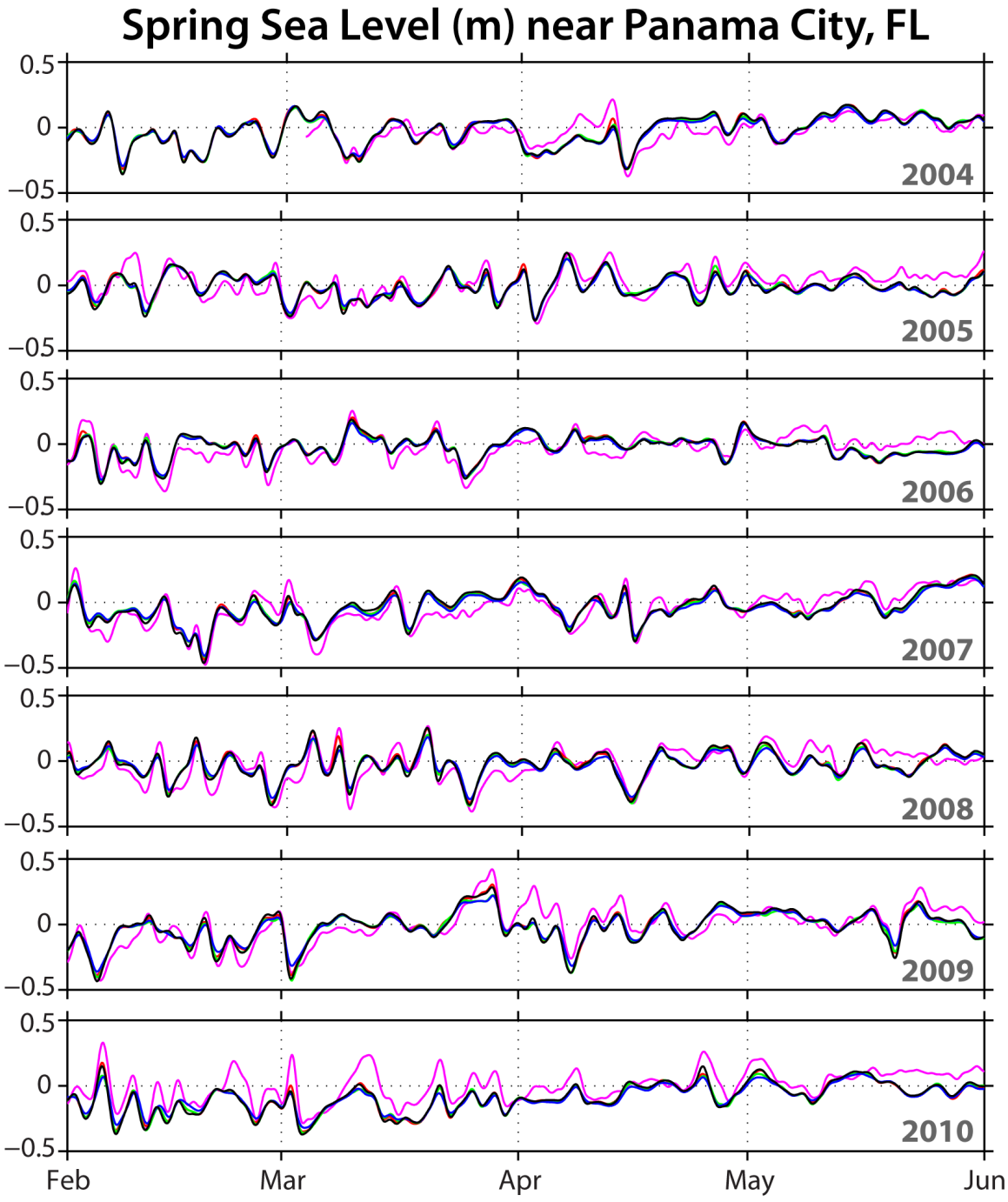

Figure 3.4: Comparison of modeled and observed springtime sub-inertial sea level near Panama City, FL. Observations are shown in pink, and red, green, blue, and black lines show modeled sea level from BBROMS simulations forced by CFSR, COAMPS, NARR, and NOGAPS, respectively.

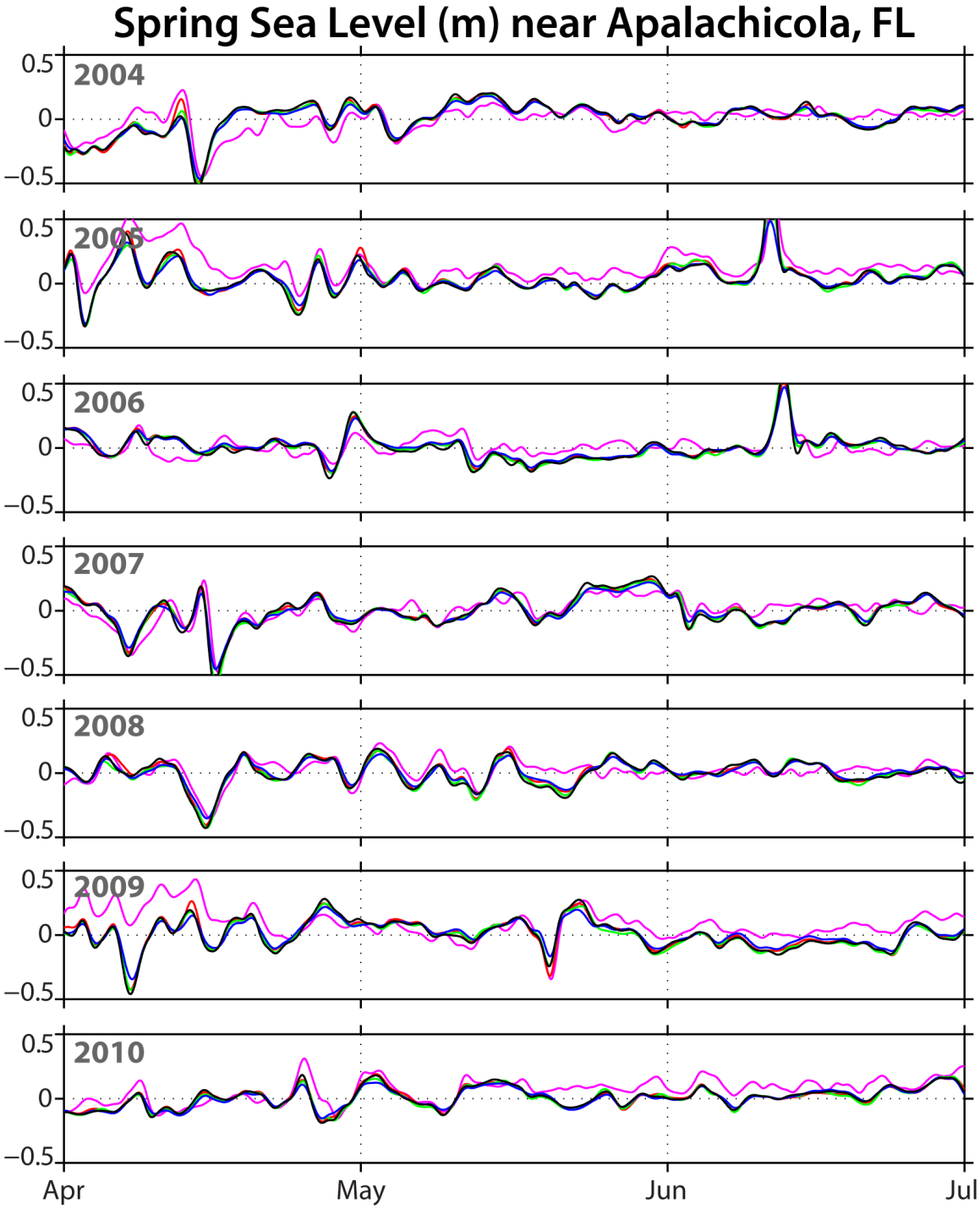

Figure 3.5: Same as figure 3.4, except for Apalachicola.

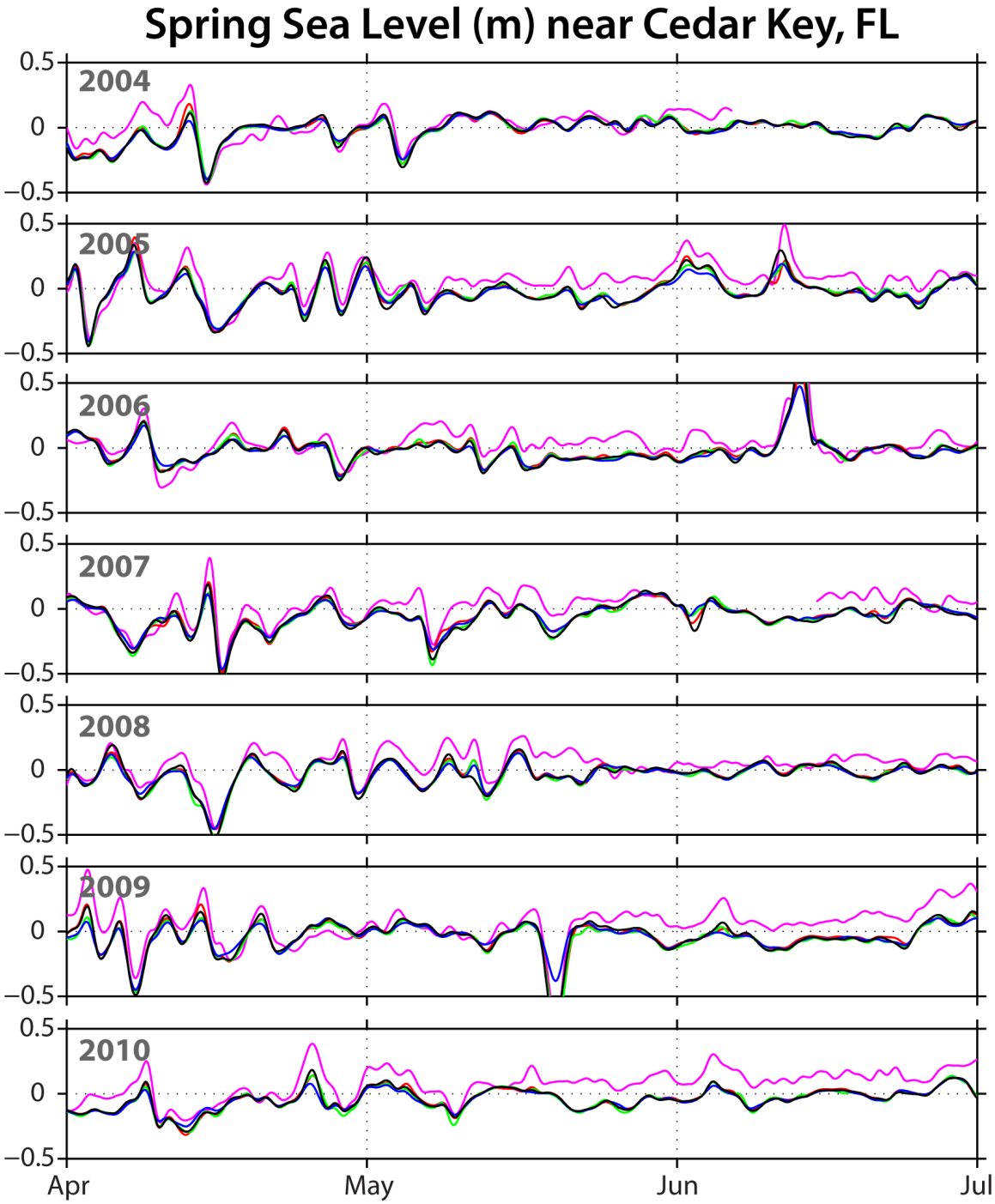

Figure 3.6: Same as figure 3.4, except for Cedar Key.

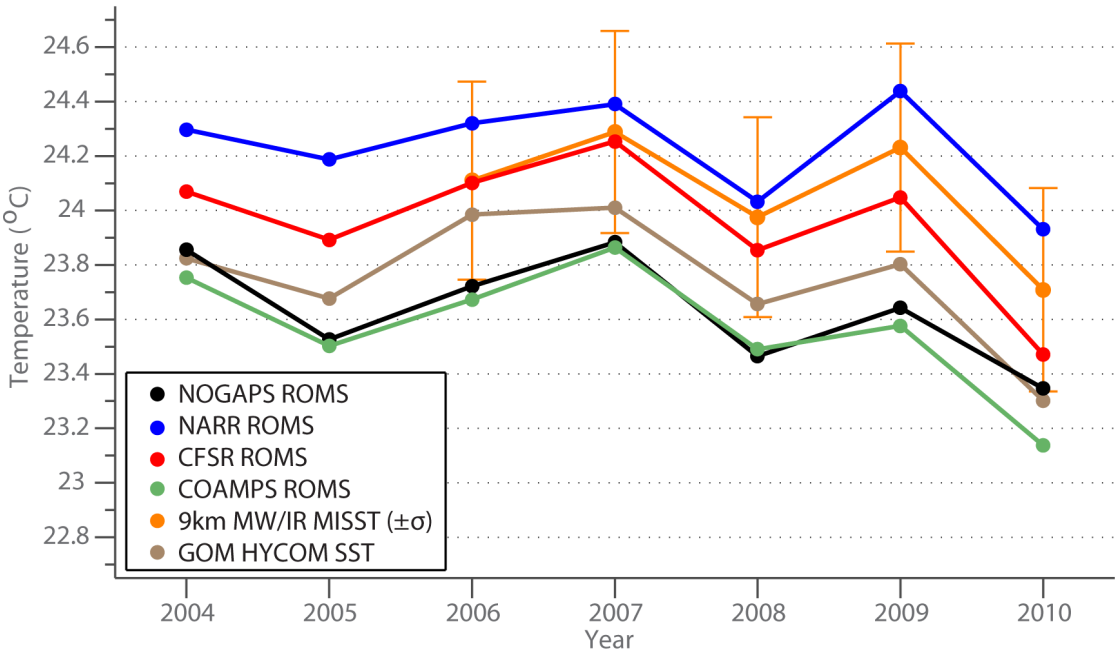

Figure 3.7: Annual mean sea surface temperatures (^{o}C) averaged across the BBROMS domain.

domain. However, the data assimilation methods used for each atmospheric model include the observed temperatures and winds at these buoy locations, which likely contributes to the improved relationships seen in this analysis. It should also be noted, however, that while the COAMPS-forced simulation produces a systematic low surface temperature bias when averaged across the domain, the linear regression fits for COAMPS at buoy locations all closely match observed values, indicating that there is no bias at these locations when compared to buoys. Furthermore, the variability is captured well by the BBROMS forced with COAMPS ($R^2 > 0.93$ everywhere). It is important to note that the heat fluxes for this model use an outgoing longwave radiation that is not calculated based on BBROMS SSTs, but rather from the MVOI surface data analysis (see Appendix A). In an effort to reduce the bias with this model, an addition of +20 W m^{-2} to the prescribed net longwave radiation is provided as a bias correction. Therefore, while this model simulation yields a slightly inferior estimate of the spatially-averaged SSTs compared to the other simulations, it performs well near buoy locations and manages to capture the variability of the

Atmospheric Forcing	Location	Slope	Intercept	R^2
CFSR	42036	1.0021	-0.1610	0.9722
	42039	1.0178	-0.1557	0.9516
	SGOF1	1.0173	-0.6935	0.9829
COAMPS	42036	1.0571	-1.2039	0.9596
	42039	1.0821	-1.4694	0.9394
	SGOF1	1.0436	-0.7526	0.9785
NARR	42036	1.0234	-0.8640	0.9719
	42039	1.0264	-0.5442	0.9547
	SGOF1	1.0278	-1.4483	0.9796
NOGAPS	42036	1.0180	-0.2467	0.9624
	42039	1.0359	-0.3620	0.9396
	SGOF1	0.9930	0.3611	0.9751

Table 3.3: Linear regression fits for SSTs between ocean model runs and moored observations.

temperatures well.

3.4.3 Currents

Velocities from each contemporaneous model simulation are compared to those observed from two bottom-mounted current profilers in 19m depth water to the southeast of St. George Sound at site N7 and further south along the same isobath at site S (figure 2.1). Through a state-funded red-tide monitoring project, and later through the Northern Gulf Institute, a bottom-mounted ADCP was deployed at site N7 on Jan 2007, with monitoring that has kept observations nearly continuous and ongoing (Maksimova 2012; Maksimova and Clarke forthcoming; Clarke and Maksimova forthcoming). The ADCP is mounted on the bottom with a blanking distance of 4 meters, and measurements have been averaged in 1 m vertical bins. Surface data contamination occurs in the upper-most 3 meters, and as such, velocities in this surface layer are removed and unavailable for analysis. The red-tide monitoring project also funded the deployment of a bottom-mounted acoustic wave and current (AWAC) profiler site S over the period from 23 April 2009 - 9 July 2010. The velocities observed using the AWAC are resolved in 1m bins from 1 m above the bottom (mab) to 16 mab, roughly 3 m below the surface. Only a few gaps occur in the data record for site N7, and a very small gap exists between deployments at site S in November 2009.

Velocities at site N7 and site S have lunar and fortnightly tides removed, are filtered to sub-inertial frequencies, and have been rotated to along-shore and cross-shore components. The along-shore axis is defined as the semi major axis of the standard deviation ellipse for depth-averaged flow, and is calculated independently for each dataset or model simulation. In similar fashion, the cross-shore currents are defined to lie along the semi minor axis of the flow. Correlations between modeled springtime along-shore / cross-shore currents and the observed currents are generally near or exceeding 0.7, indicating that the variability of the observed flow is captured well by the model simulations (figures 3.8 and 3.9). The exception is for the NARR-forced run, whose springtime correlation values fall below 0.5 in 2008 and below 0.6 for along-shore currents in 2010. The inter-quantile range (difference between the 20th and 80th percentiles) of the flow at N7 demonstrates that the variability in the observed along-shore currents ranges from as low as 5 cm s^{-1} near the bottom to almost 20 cm s^{-1} near the surface, with an inter-quantile range of the depth-averaged flow at about 10 cm s^{-1}. The inter-quantile range of cross-shore currents varies from 5-10 cm s^{-1} in 2007-2009, although 2010 shows increased cross-shore flow (particularly near the bottom) with inter-quantile range of up to 12 cm s^{-1} at 6 mab. This average range of variability is considerably larger than the means at each depth, which are at least an order of magnitude smaller on average (figure 3.10). The depth-averaged inter-quantile ranges for along-shore flow are 30 times larger than the means.

Each model tends to overestimate the strength of significantly strong flow events at site N7 by up to roughly 5-10 cm s^{-1} (25-50%). These strong forcing events occur most frequently in the up-coast (positive alongshore) direction, corresponding to the passage of cold fronts, and are particularly evident during the strong el Niño year of 2010. The overestimation is seen to occur more dramatically in the bottom half of the water column. This is evident from profiles of the upper and lower quantiles of the observed cross-shelf flow in 2010 (figure 3.10), where the variability of near-bottom flows is much larger than in other years. However, the cause of this overestimation during stronger forcing events is unclear.

The overestimation of the stronger flows is reduced at site S, where the current speeds are generally weaker overall in 2010 (the inter-quantile range is 3-15 cm s^{-1}). At this

location, the model spread is narrower and collapsed onto the observed currents (figure 3.11). The correlations remain within the same range as those observed at site N7 in 2010, with runs forced by COAMPS and CFSR exhibiting high correlations ($R > 0.8$) and the NOGAPS-forced simulation exhibiting lower correlations ($R \sim 0.66$). The NARR-forced simulation again performs the worst of all the simulations, only capturing $\sim 60\%$ or less of the variability in observed currents.

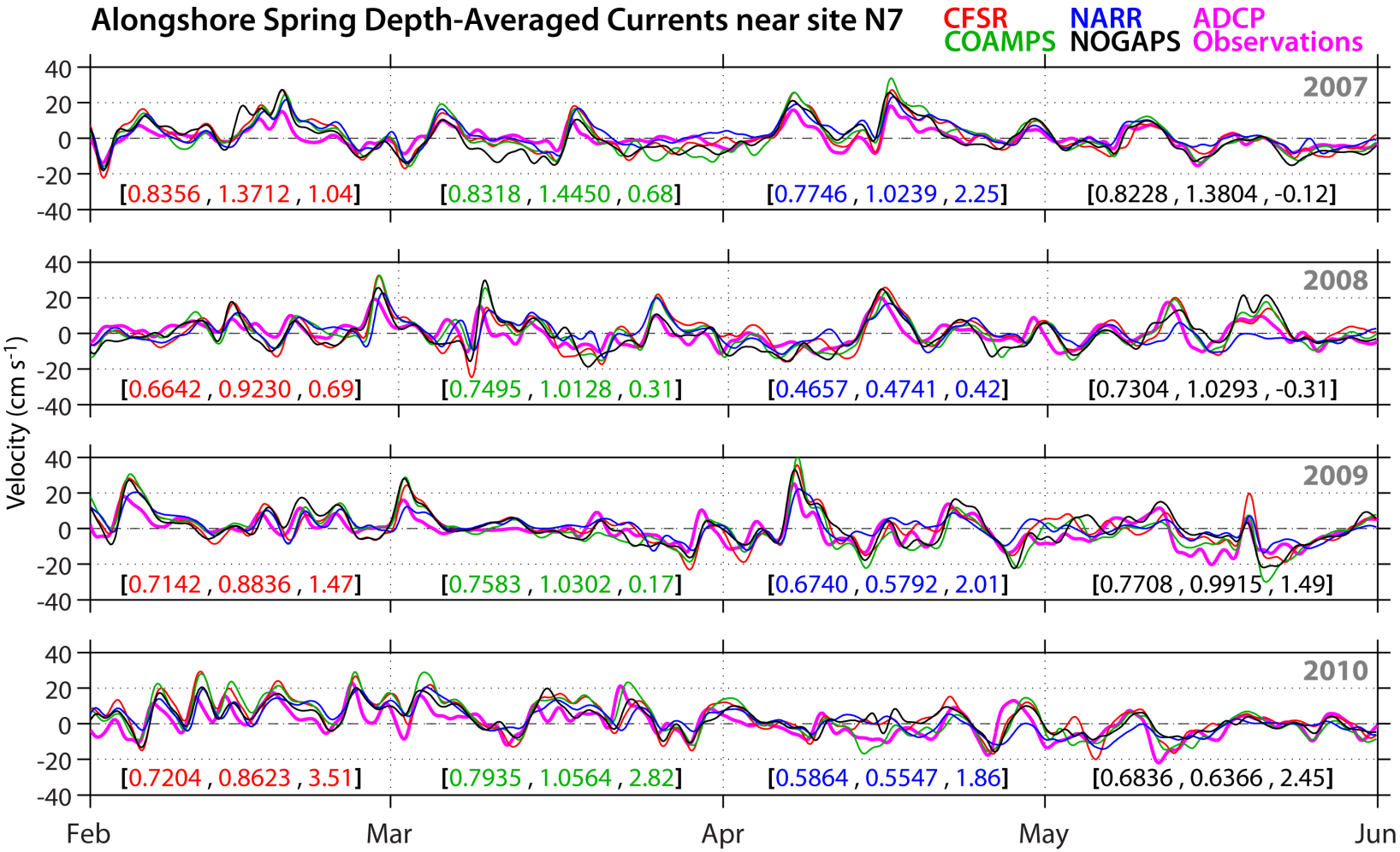

Figure 3.8: Comparison of observed and modeled depth-averaged sub-inertial springtime alongshore currents at site N7. Values in the triplet indicate the correlation R, the regression slope, and the difference between modeled mean and observed mean currents. Observations are shown in pink, and red, green, blue, and black lines show modeled sea level from BBROMS simulations forced by CFSR, COAMPS, NARR, and NOGAPS, respectively.

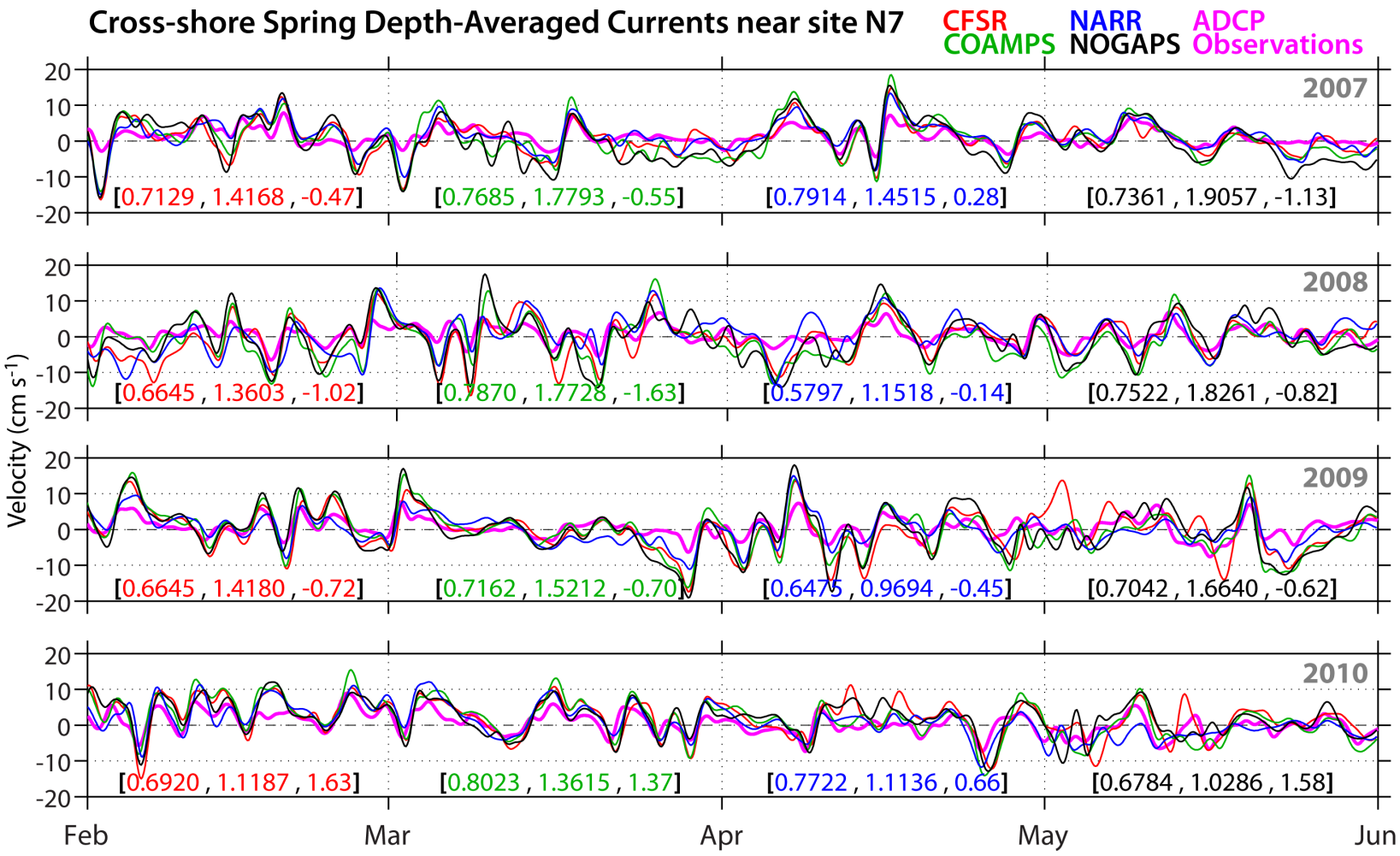

Figure 3.9: Same as figure 3.8, except for depth-averaged springtime cross-shore currents.

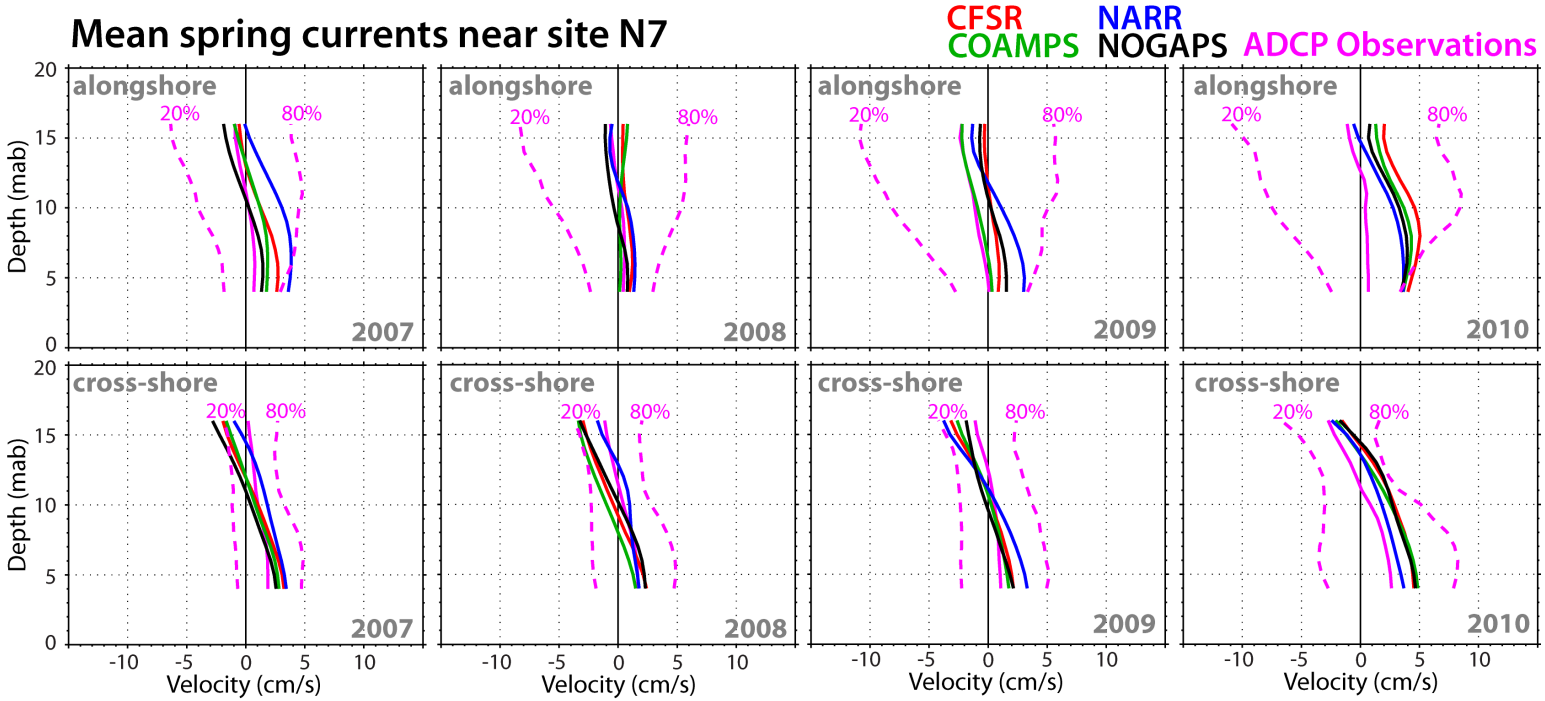

Figure 3.10: Comparison of mean observed and modeled springtime currents at site N7. Observations are shown in pink, and red, green, blue, and black lines show modeled sea level from BBROMS simulations forced by CFSR, COAMPS, NARR, and NOGAPS, respectively. The 20th and 80th percentiles of the observed flow are shown by dashed pink lines for each depth.

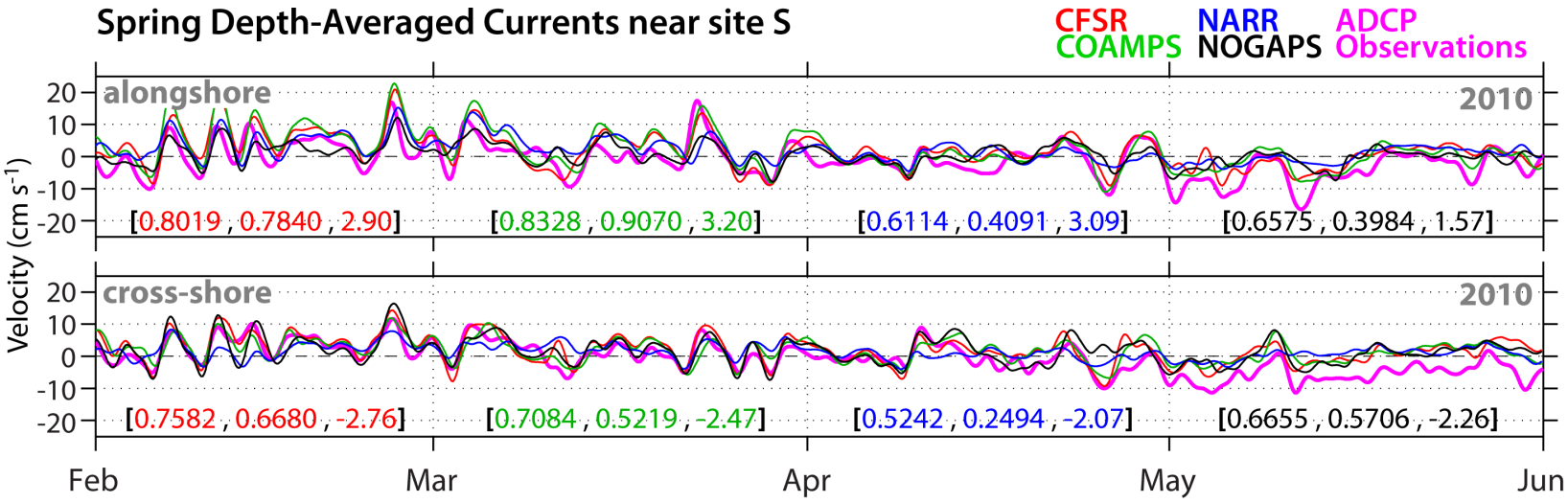

Figure 3.11: Comparison of observed and modeled depth-averaged springtime alongshore currents at site S. Values in the triplet indicate the same set of values as in figure 3.8.

3.5 Mean circulation features

This section provides a description of the dominant springtime flow features observed in the 7-year average of springtime velocities. On average, all four contemporaneous simulations reproduce several distinct features. A surface- to mid-depth concentrated jet flows northwestward along the continental slope (figures 3.12-3.14). This slope jet is not present in the simplified WFS model presented by He and Weisberg (2002b), and it flows in the opposite direction to the jet proposed by Hetland et al. (1999) and observed further south by He and Weisberg (2003). However, the northwest-flowing current seen in each BBROMS simulation is consistent with the flow provided by the open boundary conditions via the GOM HYCOM. Since He and Weisberg (2002b) neglect LC forcing during their study period of March - May, and Hetland et al. (1999) use a hypothetical LC setup, these studies do not capture the variability in LC position and extent. Furthermore, the work by He and Weisberg (2003) consider flow much further south during June 2000, which does not exclude the possibility of a northwestward-flowing slope current in the BBR during the spring months. Therefore, the strong flow offshore of the shelf break is attributed to deep ocean fluxes set by the open boundary conditions (an idea that is consistent with He and Weisberg 2003).

Adjacent to this area of northwesterly flow along the slope, there is a distinct separation in flow patterns between the circulation on the shelf and the circulation over the continental slope and deep ocean. Between the two regions, the mean vertically-averaged currents change direction by 180 degrees across a narrow region of about 15-20 km at the shelf break. This highlights that the deep ocean fluxes rarely exert their influence on the flow along the WFS (Weisberg and He 2003). Therefore, since this study is mostly concerned with the wind-driven flow on the shelf and not the flow seaward of the shelf break, which is set mostly by the deep ocean, the focus of discussion in this section will lie with those features shoreward of the shelf break.

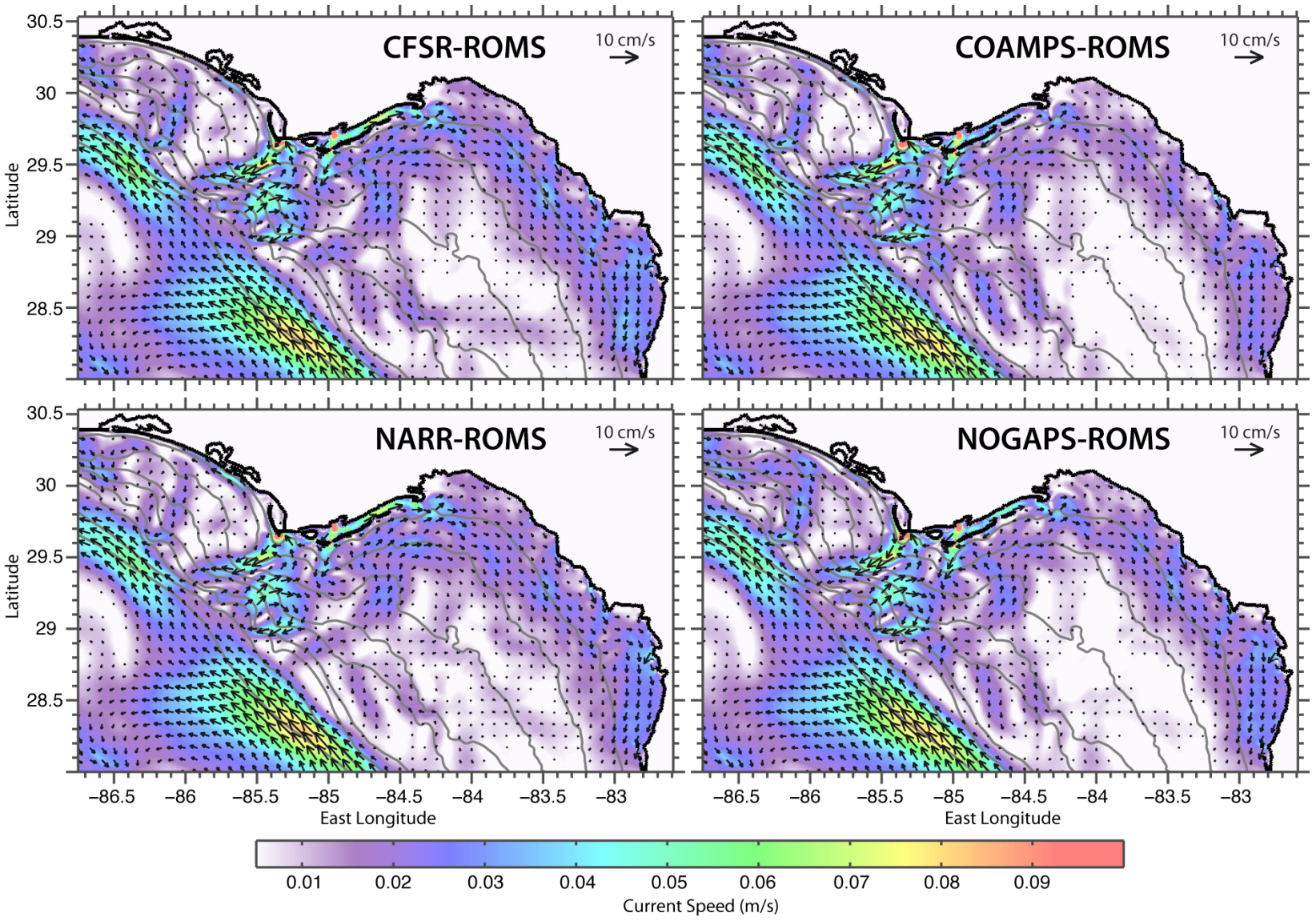

Figure 3.12: Seven-year mean vertically averaged spring velocities for each contemporaneous model run. Current speeds are in color, with velocity vectors plotted every 10 model grid points.

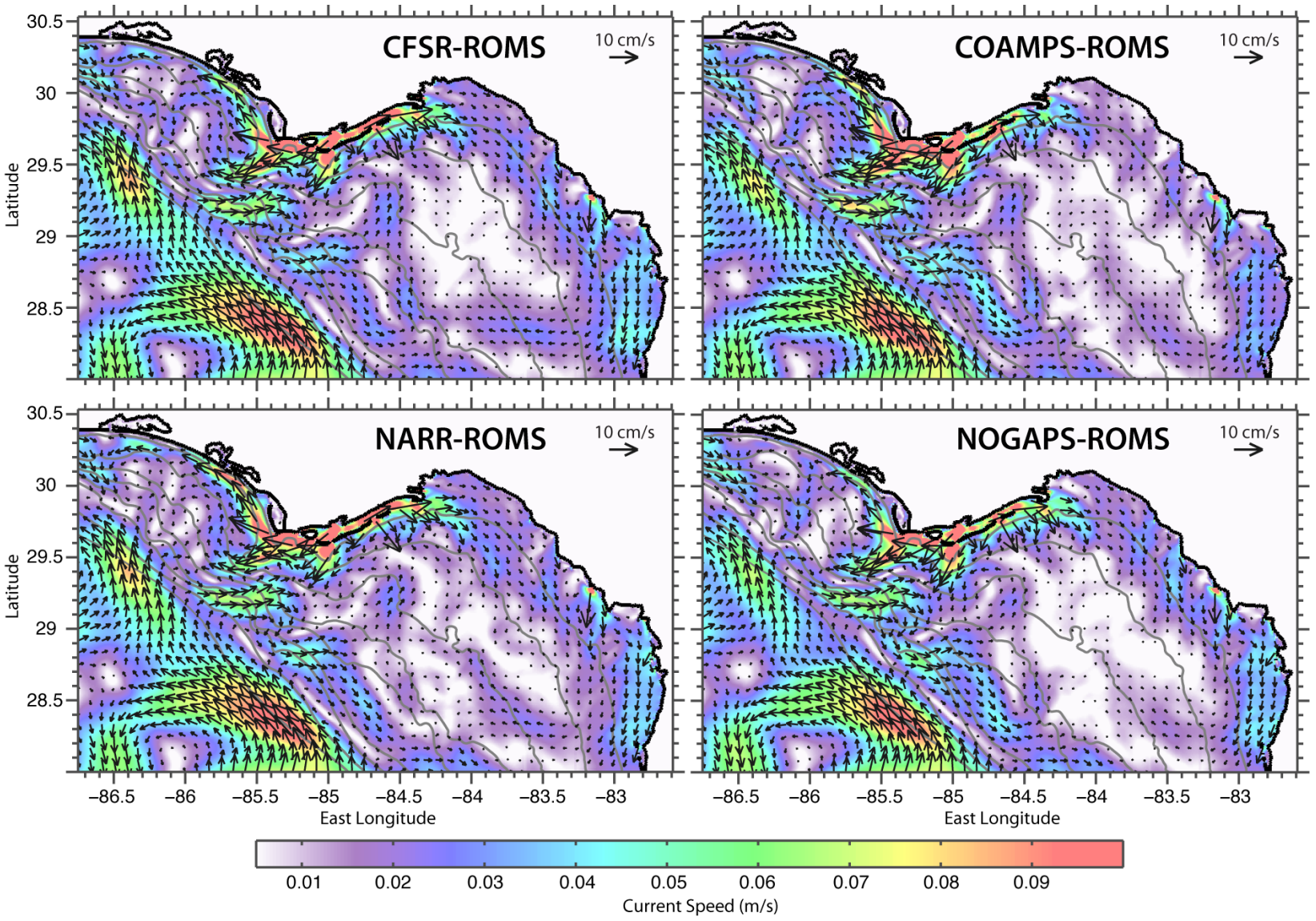

Figure 3.13: Same as figure 3.12, except for seven-year mean near-surface velocities.

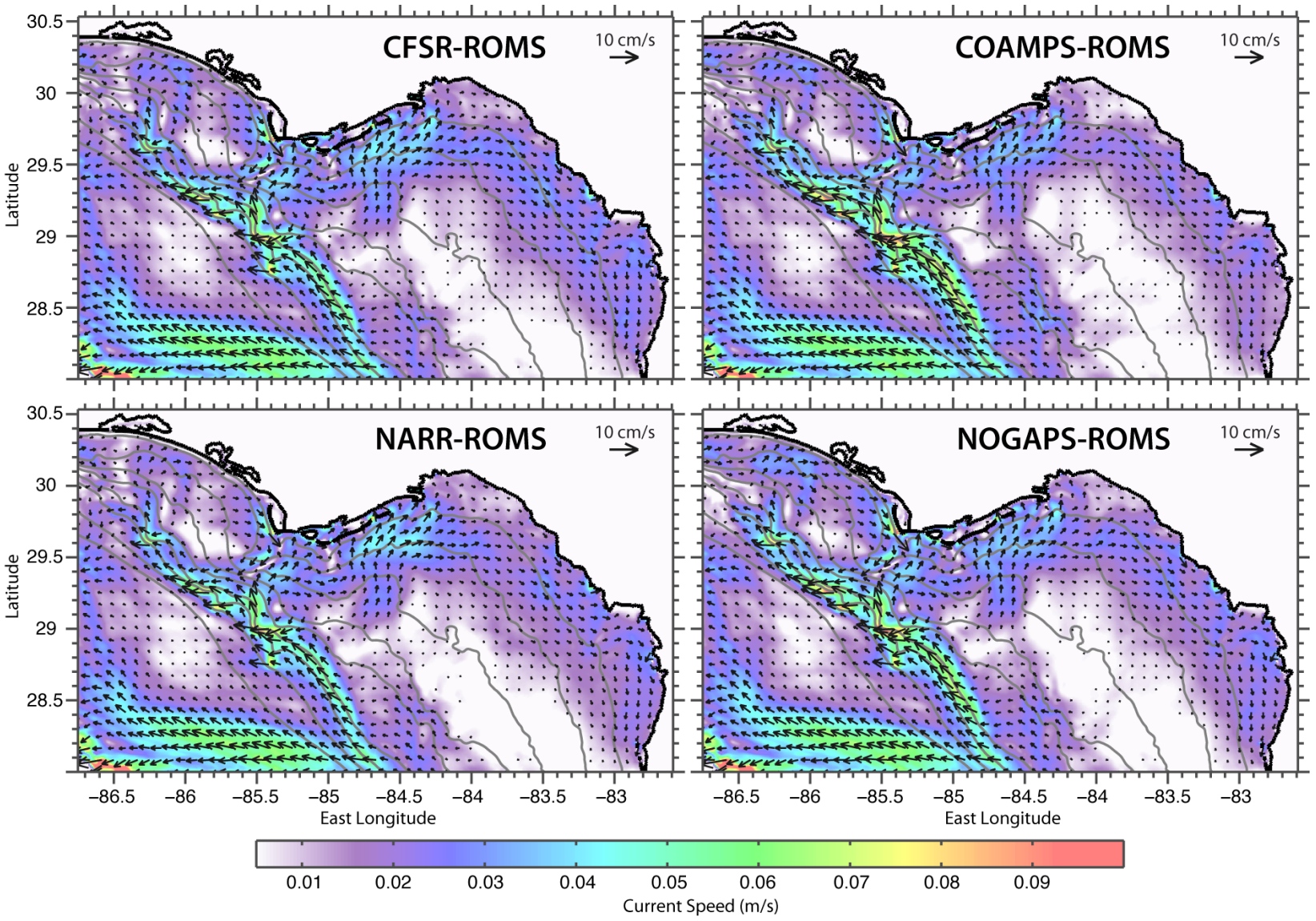

Figure 3.14: Same as figure 3.12, except for seven-year mean near-bottom velocities.

Perhaps the most striking feature of the mean vertically averaged velocities is the area just offshore of CSB and CSG. The mean flow in this area exhibits a banded structure of on-shore currents juxtaposed with areas of offshore currents. This pattern exists every year, with the mean cross-shore currents extending nearly entirely from the coastline to the shelf break. This feature is not only seen in the vertically averaged velocity fields, but also at all depths (figures 3.13 & 3.14).

Inshore and eastward of this region, close to the barrier islands that separate Apalachicola Bay from the GOM, the mean flow is cross-shore and vertically sheared, with opposing surface and bottom velocities directed offshore and onshore, respectively (figures 3.13 & 3.14). The near-surface velocity field highlights the influence of the BBR rivers to the near-coastal surface circulation, as surface velocities are directed outward from Apalachicola Bay. Due to the Earth's rotation, the less saline surface waters flow adjacent the coastline and to the right (toward the west) in the absence of northerly or westerly winds (Lentz 2012). These less saline waters are occasionally advected toward the south and east under winds from the north or west and can provide an offshore flux of waters with low salinity and high chlorophyll content over the mid-shelf (Morey et al. 2009). This southward transport of high chlorophyll water along the mid-shelf contributes to the "green river" phenomenon described by Gilbes et al. (1996) and Morey et al. (2009), which attributes the observed high chlorophyll content surface waters several hundred kilometers south along the mid-WFS to outflow from the Apalachicola River. So, while the mean surface circulation shown in figure 3.13 shows an outward flow of these buoyant surface waters, this flow is highly variable and its extent to the south and east relies on a specific combination of winds from the north or west. The mean near-bottom velocities inshore of the 20m isobath in this region are directed toward the coast, particularly at the eastern end of Apalachicola Bay, highlighting the vertical shear in the region of influence of the rivers.

Along the eastern portion of the BBR, the mean alongshore flow within the 20m isobath is mostly barotropic and directed toward the southeast, forming a coastal jet. He and Weisberg (2002b) describe a southeastward-flowing jet that bifurcates at CSB into a shelf-break jet and a coastal jet. However, the seaward component of this jet separation is not observed in the 7-year means of Feb-May circulation from each BBROMS simulation.

Instead, a coastal jet is captured, with the shelf break component dissipating immediately to the south of the region where He and Weisberg (2002b) observe a bifurcation. The dissipation modeled with the BBROMS is likely due to the spreading of the isobaths to the southeast of CSB, causing the flow to weaken via the conservation of momentum. There is an area of enhanced southeastward surface flow just shoreward of the shelf break to the southeast of the region with net cross-shore velocities, however this is not observed in the depth-averaged flow. The southeastward flow near the coast is observed at all depths, although the strength of this coastal "jet" remains fairly week (less than 5 cm/s). Velocities are very weak on average over nearly the entire mid-shelf in the widest portion of the BBR shelf where there is little bathymetric variability.

There are very little differences between the mean flow fields of each contemporaneous BBROMS simulation. All of the dominant flow features described above are present in each simulation, and the widths, directions, structure, and locations of these features all closely match. The largest difference between the model runs arises with the NARR-forced BBROMS. While the mean features of this simulation match the other simulations, it does a poor job at capturing the variability of observed currents. This is evident through the reduced correlations when compared to observed currents at site N7 and site S. Otherwise, the CFSR-, COAMPS-, and NOGAPS-forced BBROMS simulations all match closely and have correlations with observed currents that generally exceed 0.7. Therefore, the systematic weak bias in NARR wind stress yields a simulation that captures the 7-year spring mean features well, but does not accurately capture the variability of currents in the BBR. It may then be concluded that the mean spring BBR shelf circulation responds primarily to the large-scale, sub-inertial wind stress, and does not vary considerably with smaller spatial or temporal scale variability in the wind stress.

In order to ease the discussion of the variability of the flow on multiple time scales, the CFSR-forced BBROMS simulation is chosen as a representative model among the four contemporaneous simulations as it consistently provides the highest correlations when compared to the different observational data. As such, it will be the one used for discussion for the remainder of this dissertation unless specifically noted otherwise.

3.6 Variability

While the dominant mode of variability for the spring circulation occurs at synoptic time scales, there remains some interannual variability of the major shelf circulation features (figure 3.15). The dominant flow features described in section 3.5 persist from year to year, although the relative magnitudes of those features may vary. In particular, 2005, 2007, and 2010 all exhibit stronger cross-shelf flow offshore CSB and CSG. While all regions of cross-shelf flow are stronger in these years, it is the onshore-flowing regions that exhibit the most distinct enhancement. This is especially true for the onshore-flowing region to the south of St. George Island. The most pronounced flow enhancement occurs in the strong el Niño year of 2010, where the mean shelf circulation features are particularly stronger offshore of CSB and CSG and throughout the coastal jet. The slope jet is not nearly as prevalent in 2005 and 2010, and seems to be affected by cross-shelf velocities as an extension of the onshore flow to the south of CSB. Contrastingly, the coastal jet vanishes in the spring mean for 2008 and 2009.

It is demonstrated in section 3.2.2 that the dominant frequency of wind stress variability occurs at synoptic scales during the spring season, mostly in association with atmospheric frontal passages (cold fronts). Indeed, figure 3.2 displays that the spring winds originate more frequently from the eastern quadrants. Winds originating from the northwest cannot be neglected, however, as these post-frontal winds are often stronger, and may actually occur as frequently as easterly winds in some years (i.e. 2006 and 2010). The mean depth-averaged flow during each wind regime may be calculated, then scaled by the percentage of time that the wind originated from that respective quadrant. Then, if it is assumed that the ocean responds linearly and instantaneously to winds from each quadrant, this resulting picture is one that demonstrates that the two dominant flow patterns are those when the wind originates from either the northwest or southeast quadrants (figure 3.16). The mean scaled flow during northeasterly winds is very weak in comparison to flow during winds from the southeast or the northwest, even though the winds quite frequently originate from this quadrant. As could be expected from the small percentage of time that winds originate from the southwest, the mean scaled flow is much weaker during winds from this quadrant than from any other direction.

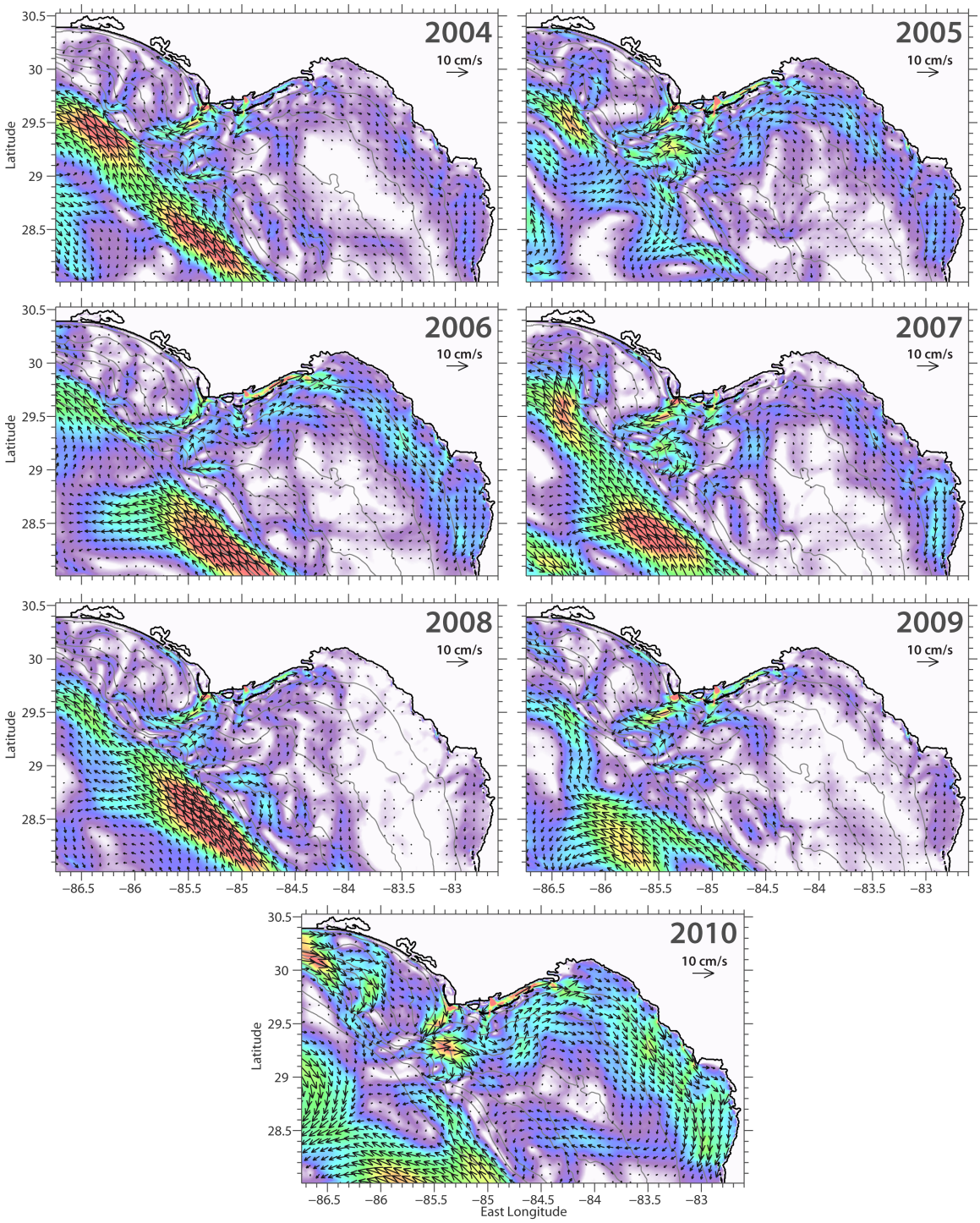

Figure 3.15: Yearly mean springtime depth-averaged velocities for the CFSR-forced BBROMS simulation. Colors represent the current speed, and arrows depict the mean depth-averaged velocities, plotted every 10 model grid points.

The scaling of these conditionally-averaged fields provides an understanding of the impact of both the frequency and strength of various flow regimes, indicating that the two dominant wind regimes are those from the northwest and from the southeast. However, the actual speeds of the currents during each regime are not retained upon the scaling of the flow fields. Therefore, the true averages are calculated for the flow during each of the two dominant wind regimes, which yields the two main flow patterns during the springtime circulation (figure 3.17). Averaging the spring velocities when the winds are northwesterly (upwelling-favorable) yields a strong southeast-directed shelf flow that is enhanced over three regions offshore of CSB and CSG. These areas correspond with the areas exhibiting mean cross-shelf flow in figures 3.12-3.14. Averaging the spring velocities when the winds are southeasterly (downwelling-favorable) yields a weaker northwest-directed shelf flow and slope jet. The slope jet is not visible for flow during northwesterly winds. Over the mid-shelf, velocities during each wind regime flow along isobath and roughly opposite to each other, although velocities are slightly weaker during southeasterly winds.

By averaging the two dominant flow patterns (the average of the flow during southeasterly winds and during northwesterly winds), a depth-averaged flow field is produced in which all of the features present in the full spring mean are retained (compare figure 3.18 to figure 3.12). That is, the cross-shelf flow offshore of CSB and CSG, the southeastward-flowing coastal jet, and the northwestward-flowing slope jet are all present in the conditionally-averaged mean flow. Thus, the cross-shelf velocities offshore CSB and CSG and the coastal BBR jet are simply the rectification of two asymmetric, oscillating flows during upwelling-favorable and downwelling-favorable winds. The flow during northwesterly winds is enhanced over the region from CSB shoal to CSG shoal. This flow enhancement is not seen for flow during southeasterly winds. Thus, upon averaging the two together, the residual is directed mostly cross-shore. A similar rectification occurs in the coastal jet, although the flow here is directed mostly along-isobath during both wind regimes, and it is simply the higher velocities of the flow during northwesterly winds that skews the mean toward flow from this direction. The mean flow along the mid-shelf of the BBR is weak (figures 3.12 and 3.18), but velocities are stronger during winds from each individual direction (figure 3.17). Thus, the weak flow seen here in the mean is simply just due to the oscillating flow

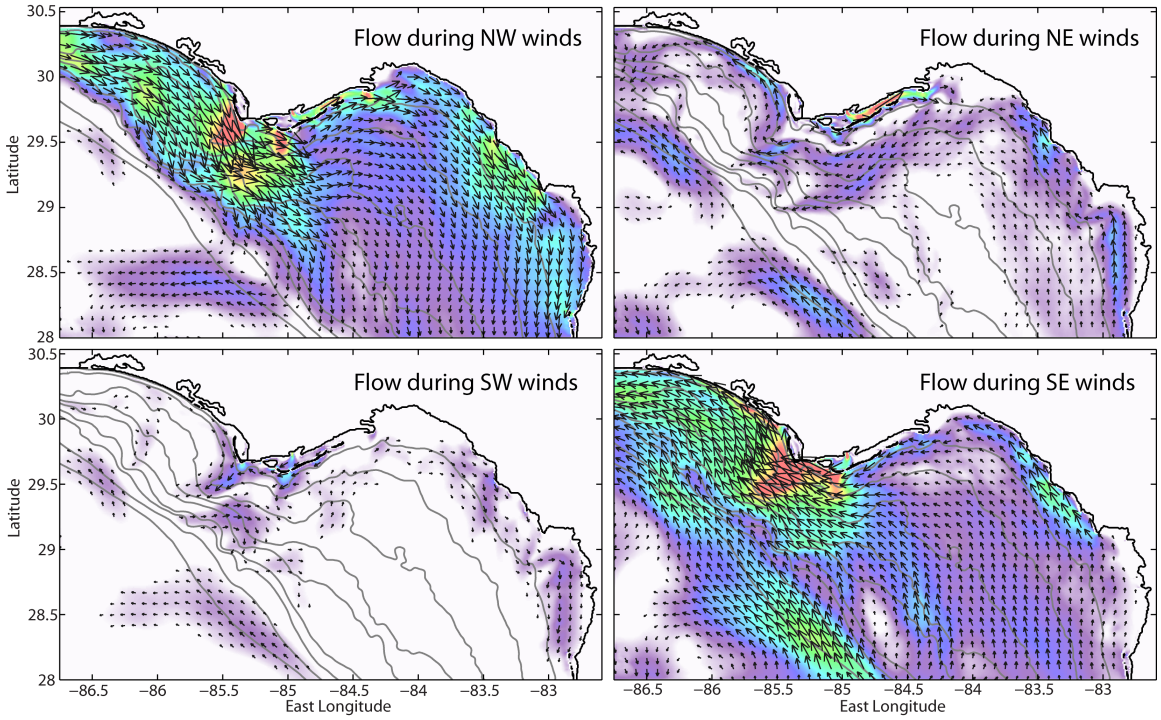

Figure 3.16: Conditionally-averaged flow fields for flow during each wind regime. Averages are calculated over all times during Feb-May (for all 7 years) when the wind originated from each quadrant respective quadrant. Averages are then scaled by the percentage of time that the winds originated from that quadrant over the entire 7-year spring period. Scale arrows are not given as the scale value is arbitrary.

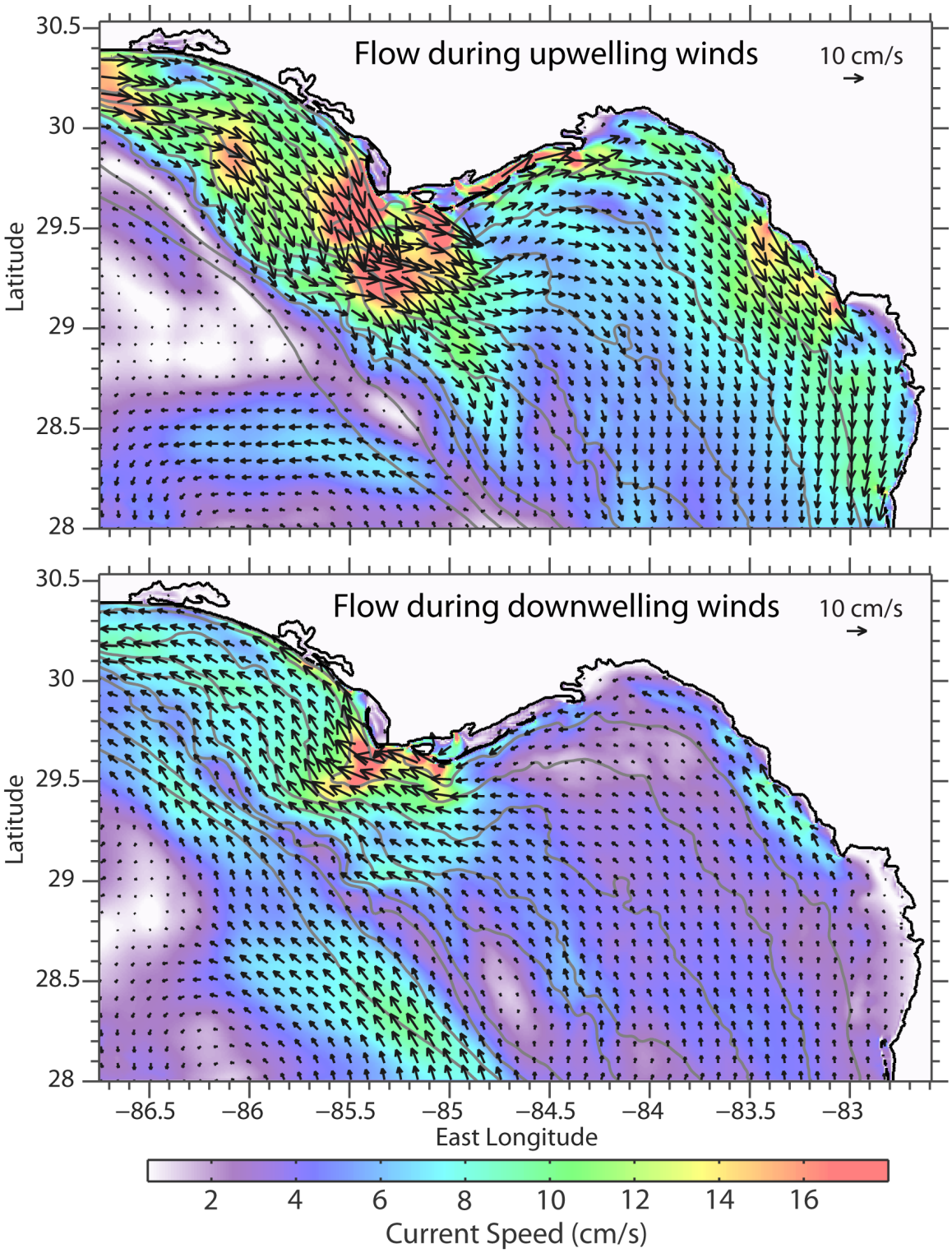

Figure 3.17: Same as figure 3.12, except for flow only during (top) upwelling-favorable winds or (bottom) downwelling-favorable winds.

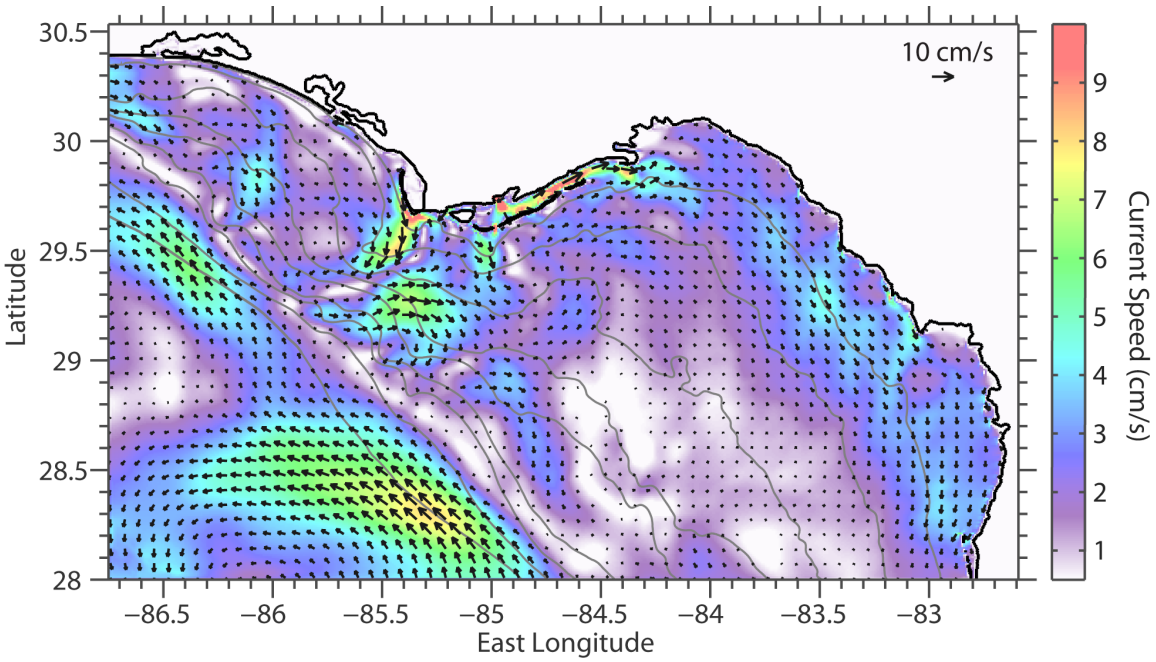

Figure 3.18: Same as figure 3.12, except for flow only during both upwelling-favorable and downwelling-favorable winds.

that is of nearly equal strength, but opposite directions.

3.7 Summary

The primary forcing mechanism of the BBR shelf waters during the springtime is the local wind stress. The springtime wind stress' dominant variability occurs at synoptic frequencies in association with the passage of cold fronts. The winds are predominantly of easterly origin, yet winds from the northwest quadrant can occasionally be as frequent as winds from either the northeast or southeast. The northwesterly winds are typically stronger than winds from any other quadrant. Over the BBR, northwest and southeast winds are upwelling-favorable and downwelling-favorable, respectively.

Four contemporaneous ocean model simulations are obtained by using different atmospheric products of varying spatial and temporal resolution as surface forcing for the models. There is very meager contrast between each of the contemporaneous model simulation's 7-year mean velocity maps (figures 3.12 - 3.14), and the resulting circulation patterns produce

features that match the observed sea level, surface temperatures, and currents well. The exception to this general agreement is for the model forced with NARR, which reproduces observed sea level, observed surface temperatures, and mean depth-averaged flow features well, but is unable to capture the variability of the observed currents. This is undoubtably due to the systematic weak bias in these winds, which produce a corresponding circulation that does not have the same variability as the observed circulation. For the remaining simulations, there is also relative agreement between modeled and observed currents at site N7 and site S. Therefore, while small-scale, high-frequency variations in the wind stress occur between the different atmospheric forcings, they are of limited importance to the mean shelf circulation features. It may then be concluded that the circulation on the BBR shelf responds to the large-scale, sub-inertial wind stress, and not to smaller temporal or spatial scale variations of the winds. This is consistent with previous results assessing the ocean's response to wind stress at discrete observational locations in the BBR (i.e. Marmorino 1983; Clarke and Brink 1985; Mitchum and Clarke 1986; Maksimova 2012).

There are two dominant flow regimes during the springtime. These consist of flow during winds that originate from the northwest or from the southeast, or during phases of upwelling or downwelling-favorable wind stress. While winds may frequently originate from the northeast quadrant, their affect on the mean depth-averaged flow is shown to be minimal, as the average flow during winds from either the northwest or southeast recover all of the dominant flow features seen in the full spring mean circulation. Winds from the northwest are stronger, driving correspondingly faster southeastward-directed currents. This flow is enhanced and is directed cross-shore over areas where the isobaths undergo tight curvature offshore of CSB and CSG. Southeasterly winds drive a weaker shelf circulation, where the flow is enhanced only over one small area just offshore of CSB. The result of combining these two asymmetric, yet opposite flows is a rectification of the flow leading to net cross-shore velocities in the region of flow enhancement during northwesterly winds. Therefore, the interannual variability in the flow features that is observed is a direct result of the interannual variability in the low-frequency, large scale wind stress over the BBR.

In the following chapter, the mechanisms by which the flow is able to cross isobaths is investigated. This leads to a discussion of the implications that the cross-shelf transport

and its variability has on gag recruitment in the BBR.

CHAPTER 4

TRANSPORT MECHANISMS IN THE FLORIDA BIG BEND REGION

The aim of is chapter is to provide an understanding of the mechanisms by which the cross-isobath movement is enhanced during southeastward flow and limited during northwestward flow. This is done using simple physical arguments relating to the vorticity of the flow, and by use of a Lagrangian particle advection model. The advected particles are used not only to describe the vorticity characteristics of the flow, but also as a very basic proxy for pelagic, passive gag larvae.

4.1 Introduction

The mean springtime circulation on the BBR shelf exhibits distinct areas of cross-shore flow in the proximity of tightly-curving isobaths. This flow arises due to the asymmetric response of the shelf circulation to oscillating upwelling- and downwelling-favorable winds. In particular, the stronger flow during upwelling-favorable winds is able to cross isobaths, whereas flow during southeasterly winds does not. Castelao and Barth (2006) provide a simple understanding of the mechanisms by which a coastal jet is able to separate from a cape during upwelling-favorable winds and move offshore. They demonstrate, through the conservation of potential vorticity, that the flow is able to cross isobaths under a variety of regimes that depend on the geometry of the cape and the magnitude of the wind forcing. In all cases, they find strong flow to be a prerequisite for the separation of the coastal jet from the cape. However, the separation increases when the square of the internal radius of deformation is close to the square of the radius of curvature of the bank. The ratio between

these two length scales (the Burger number), has important implications to the ocean's response to significant wind forcing. When the jet does separate from the cape, Castelao and Barth (2006) find the dominant balance to be between the ageostrophic and the nonlinear parts of the flow, causing an acceleration of the flow offshore when encountering the shallow depths of the cape. Larger asymmetry in the cape geometry increases the offshore transport.

Near-steady upwelling-favorable winds are commonly observed off the coast of Oregon, where Castelao and Barth (2006) find application for their study. However, the springtime winds in the Florida BBR do not persist from one particular direction for a significant period of time. Therefore, the work in this dissertation must consider the effect of a wind that oscillates from phases of upwelling to phases of downwelling, and vice versa. Moreover, the geometry of isobaths offshore of CSB and CSG in the BBR exhibit multiple areas of varying lengths and directions of curvature radii, which can lead to a much different modal response of the shelf waters than off the coast of the Pacific Northwest United States. Mitchum and Clarke (1986) demonstrated that the WFS exhibits barotropic fluctuations in response to low-frequency wind forcing. However, due to the latitude and general length scales of the Oregon or Northern California shelves, Clarke and Brink (1985) found the response of the ocean in that region of the world to have much more baroclinicity. The BBR represents an area where the concepts from these previous works can be applied to a more complex and realistic ocean setup, in order to gain an understanding of the physical processes governing cross-shore movement in the BBR and its implications on the advection of larvae across the shelf. Therefore, the findings of the previous chapter provoke the following questions: what allows flow to cross isobaths in one direction, but not in the opposite direction? Is the cross-shore flow observed by the springtime mean velocities capable of providing the necessary transport from the shelf break to the coast for gag larvae? If so, do preferred pathways exist for this onshore transport? These questions are approached in the following sections using simple physical arguments and by use of a Lagrangian particle advection model.

4.2 Vorticity characteristics of the flow

Flow that crosses isobath must exhibit some change in its absolute vorticity. This may occur as a modification to the relative vorticity, latitudinal movement, or as a stretching or tilting of the fluid column. If the flow is barotropic, it conserves its potential vorticity (PV) through the relationship

$$\frac{d}{dt}\left(\frac{\zeta + f}{h}\right) = 0 \tag{4.1}$$

where $\zeta = \partial v/\partial x - \partial u/\partial y$ is the relative vorticity of the flow, f is the Coriolis parameter, and h is the ocean depth at a given location. Consistent with Clarke and Brink (1985), and since the dominant flow features seen in section 3.5 appear throughout the water column, the shelf response to fluctuating large-scale, low-frequency wind forcing over the BBR may be assumed to be barotropic. The Burger number is often used to describe the baroclinicity of the flow. That is,

$$Bu = \frac{N^2 H^2}{f^2 L^2} = \left(\frac{R_D}{R_c}\right)^2 \tag{4.2}$$

where L is a length scale defined to be the radius of curvature of the topography, R_c, $R_D = NHf^{-1}$ is the Rossby radius of deformation of the flow, $N = [(-g/\rho_0)\,\partial\rho/\partial z]^{1/2}$ is the Brunt-Väisälä (buoyancy) frequency, ρ is the density, ρ_0 is a constant reference density, H is the undisturbed water depth, and z is the vertical coordinate. The Burger number, Bu, therefore characterizes the interplay between the stratification, shelf geometry, latitude, and characteristics of the forcing (Dukhovskoy et al. 2009). Thus, if $Bu \ll 1$, the flow response can be considered to be barotopic, whereas $Bu \gg 1$ implies strong baroclinicity to the ocean response. Indeed, for springtime flow over the BBR, the mean Burger number over the shelf (shallower than 200m) is $\mathrm{O}(10^{-3}) \ll 1$, indicating that the shelf response should indeed be of barotropic nature (consistent with Clarke and Brink 1985).

Flow that is barotropic may conserve its PV by following contours of f/h. However, if this constraint is broken by an abrupt change in h, some relative vorticity must be introduced in order for conservation to occur. Therefore, according to equation 4.1, it is the relationship between ζ and f that determines if the flow will conserve its PV when it encounters a change in depth. In order to demonstrate the relationship between ζ and f,

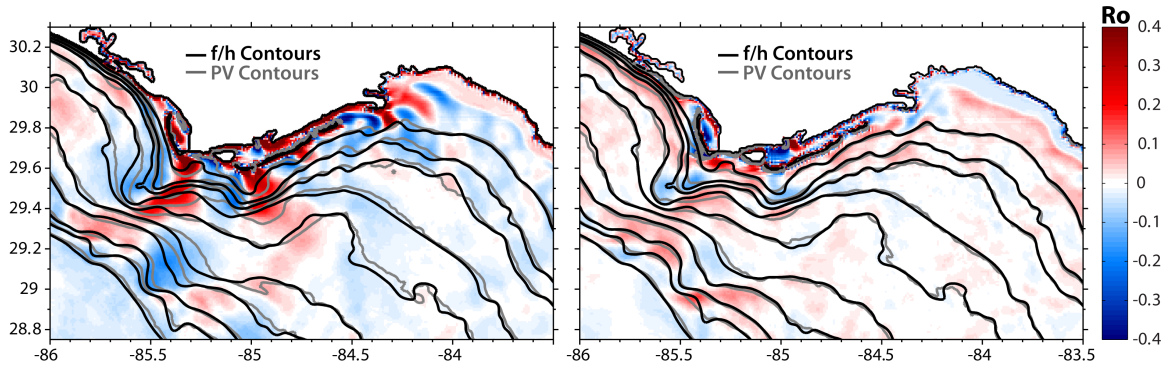

Figure 4.1: Color represents the Rossby number for flow during northwesterly winds (leftt) and during southeasterly winds (right). Grey contours show the potential vorticity of the flow and black contours are f/h.

the Rossby number may be defined in similar fashion to Castelao and Barth (2006) as

$$Ro = |V| / fL = |V| / fR_c \sim \zeta / f \tag{4.3}$$

where V is a velocity scale of the flow and L is again a length scale defined to be the radius of curvature, R_c. That is, as $|Ro| \to 1$, the relative vorticity plays an increasingly large role in governing the flow. This condition occurs during strong flow ($|V|$ large), or for flow over tightly curving isobaths (R_c small). For weaker flow ($|V|$ small) or flow over gently curving isobaths (R_c large), $|Ro|$ is small and so Coriolis dominates the relationship given by 4.3. In this latter case, the flow should follow contours of f/h. At any given location on the shelf, f and $|R_c|$ do not change, so the greater magnitude of Ro for northwesterly winds in figure 4.1 indicates that the stronger flow during these winds is more likely to cross isobaths and therefore induce relative vorticity in the flow. Given the response seen by Castelao and Barth (2006), increased $|Ro|$ for flow during northwesterly winds provides a greater potential for it to separate from its original isobath.

It is possible to use the arguments of PV conservation to explain the flow features during the two dominant flow regimes discussed in section 3.6, if it is assumed that the flow during each wind regime conserves PV. For example, when the southeast-flowing current during northwesterly winds encounters the shallow waters of the CSB shoal (decreasing h), it must turn to the right (in the offshore direction) in order to add negative ζ to the flow. The rapidly

curving isobaths in this area cause the offshore-flowing current to quickly encounter deeper water (increasing h), which then requires the flow to induce a positive ζ and consequently turn back to the left (onshore). Due to the geometry of the shelf offshore CSB and CSG, this process repeats twice more before the flow is finally able to adjust and flow along-isobath over the wider, gently-curving shelf east of N7. The areas with intersecting and separating of contours of f/h and PV in figure 4.1 during this flow regime indicate the locations where PV-conserving flow can be expected to cross isobaths. The crossing of isobaths occurs in conjunction with the change in sign of Ro. Since Ro can only change sign with ζ, figure 4.1 depicts this example of PV-conserving flow during northwesterly winds.

Flow during southeasterly winds is weaker, thereby providing smaller magnitudes of Ro (figure 4.1). This weaker northwestward flow is then able to quickly adjust to the tightly curving isobaths, reducing the need to add significant relative vorticity to the flow in order to conserve its PV. For this reason, the contours of f/h closely match contours of PV during this flow regime, with the exception of the region of very tight curvature over CSB shoal. Thus, flow during this wind regime can also be expected to conserve its potential vorticity, with weaker flow that reduces the potential for offshore movement.

Incongruity between contours of PV and f/h suggests, but does not necessarily indicate, that the flow indeed conserves its PV when crossing isobaths. Equation 4.1 may be evaluated at two consecutive time steps t and $t + \Delta t$, such that

$$\left(\frac{\zeta + f}{h}\right)\Big|_t = \left(\frac{\zeta + f}{h}\right)\Big|_{t+\Delta t} \tag{4.4}$$

or

$$\frac{\zeta + f}{h} = \frac{(\zeta + \Delta\zeta) + f}{h + \Delta h} \tag{4.5}$$

which, assuming changes in f from one time-step to another are negligible (or f-plane flow), simply reiterates that flow moving over sharply changing bathymetry must induce some relative vorticity in order to conserve its PV. Rearranging equation 4.5 reveals the relationship

$$\frac{\Delta h}{h} = \frac{\Delta\zeta}{\zeta + f} \tag{4.6}$$

which says that the fractional change in depth of the flow from one time step to another should be balanced by a corresponding change in relative vorticity if PV is indeed conserved.

By tracking the evolution of the depth and relative vorticity in the flow through time, it is possible to test if this relationship holds, and therefore to test if the flow indeed conserves its PV. This task will be accomplished using a Lagrangian particle advection model.

4.3 Lagrangian particle advection model

Lagrangian particle advection models can be used for a variety of applications to geophysical fluid flows. This study beckons the use of a particle advection model not only to track the evolution of potential vorticity in the circulation, but also as a proxy for the advection of gag larvae across the shelf. By advecting passive particles in the circulation, one may obtain an understanding of the pathways by which materials are able to arrive onshore, along with the temporal variability in their onshore transport. Then, by using the concepts outlined in section 4.2, the physical mechanisms by which particles are transported across the shelf may be assessed.

For this study, the Larval Transport Lagrangian Model (LTRANS; see North et al. 2008; Schlag et al. 2008) is used to identify primary pathways for onshore transport of passive Lagrangian particles. LTRANS predicts the movement of particles by using advection, subgrid scale turbulence, and particle behavior (although not used in this experiment). The external time step of the model is the output frequency of the hydrodynamic BBROMS simulation (3 hourly), and LTRANS uses an internal time step of 15 minutes to track the evolution of particle positions. With a time step of 15 minutes, the particles are unable to be advected across an entire grid cell in one time step. The hydrodynamic fields are then interpolated to provide a highly resolved velocity field for particle advection. Details of the interpolation and advection procedures for this configuration may be found in Appendix C.

4.4 Transport mechanisms and particle pathways

The basic relationships that should hold if the flow conserves its PV are demonstrated in section 4.2. In particular, the time evolution of a parcel of water flowing in a PV-conserving system should follow the relationship given by equation 4.6. It is possible to track the evolution of depth and relative vorticity along Lagrangian particle paths to assess whether or not this relationship holds. For this experiment it is assumed that the flow is barotropic,

and as such a Lagrangian particle's vertical position is considered to be inconsequential to the result. Each particle may then be considered a parcel of water covering the depth of the fluid column.

The time-evolution of each side of relationship 4.6 is calculated for each particle. Then, the average of each are calculated within $0.05^o \times 0.05^o$ bins across the BBR modeling domain. When contoured together (figure 4.2), the mean springtime flow over the BBR shelf is seen to be generally PV-conserving. The co-location of areas of high and low values of $\Delta\zeta/(\zeta+f)$ and $\Delta h/h$ demonstrates that cross-shore movement of the flow is compensated by the addition of relative vorticity of the same sign and magnitude. Indeed, both the signs and the magnitudes of each side of 4.6 match well across all the areas in which significant cross-shore flow is observed in figure 3.12. The exception to this agreement in figure 4.2 occurs in areas where there is commonly freshwater outflow from the Apalachicola River (i.e. to the west of CSB and at the west end of Apalachicola Bay). Buoyant riverine water frequently exists in these areas, enhancing the stratification and therefore causing the barotropic assumption in equation 4.1 to break down. For these cases, the depth of the density layer should be tracked, and not the depth of the entire water column. That being said, there is agreement between both sides of equation 4.6 in the areas where considerable cross-shore flow occurs, which are the main areas of interest for this study. It is therefore concluded that the barotropic flow on the BBR shelf conserves its potential vorticity, which allows for cross-shore movement during strong northwesterly wind events.

While the ability of PV-conserving flows to allow for cross-shore movement of particles has been demonstrated, this study also seeks to determine the distribution of particles in the domain over their advection period, and to examine the variability in their spatial distribution. With over 1 million particles, it is difficult to determine the preferred locations of advection by simply looking at the individual particle trajectories. Therefore, the domain is divided into $0.1^o \times 0.1^o$ boxes, and the percentage of all particles to pass through each individual box at any time during their entire advection period is calculated (henceforth referred to as particle "density"). This calculation allows the preferred particle advection pathways to be deciphered. Figure 4.3 shows the density of all particle trajectories over the entire 7-year advection period. It is not surprising that the highest percentage of

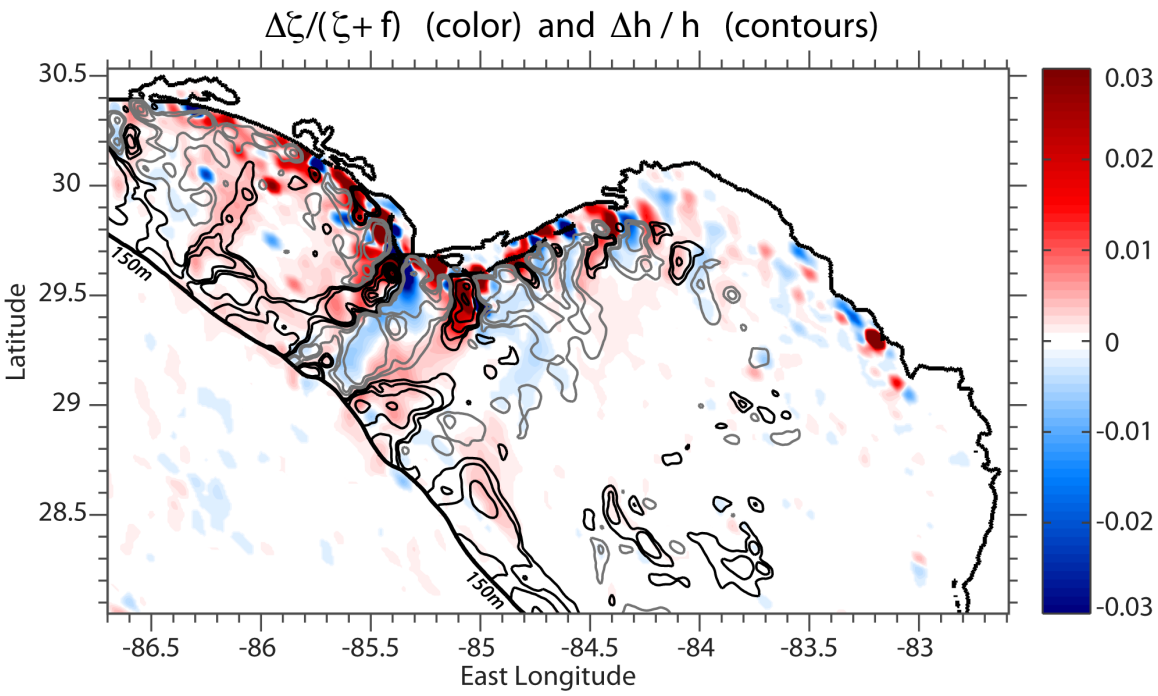

Figure 4.2: Colors denote mean values of $\Delta\zeta/(\zeta + f)$ and contours depict mean values of $\Delta h/h$. Values are calculated based by averaging values at each location following all 1,467,648 particle trajectories.

particles appears along the shelf break, as this is the location where the particles are seeded and are able to be transported in the slope jet. It is evident that the slope jet provides the primary flow of particles, as the percentages are skewed toward higher values along the shelf break in the northwest portion of the domain compared to the shelf break near the southern boundary. Due to this northwestward flow, 38.65% of all particles leave the domain through the western boundary, while 17.3 % leave through the southern boundary. This demonstrates that, while half of the particles advected remain inside the domain, the primary location for particles to exit the domain is through the western boundary via the northwestward-flowing slope jet. However, there are occasional bursts of particles that are able to cross isobath and move onshore (or offshore) during upwelling-favorable winds, via the mechanisms previously discussed using the conservation of PV. This reiterates the fact that southeasterly winds (and hence northwestward flow) are more frequent during the spring, but the northwesterly winds (southeastward flow) can contribute significantly to the

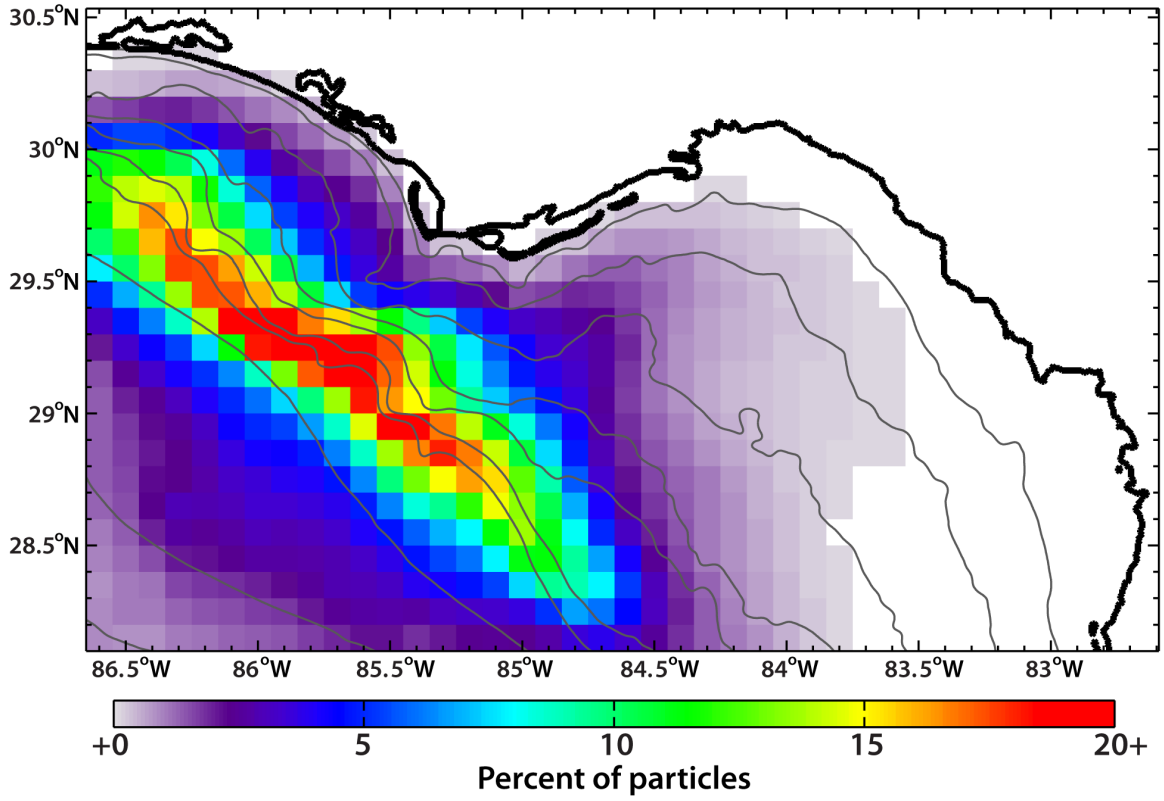

Figure 4.3: Density of particles advected through each $1/10^o$ x $1/10^o$ box with the LTRANS simulation using ocean model fields from the CFSR-forced BBROMS. Colors denote the percentage of all particles over the 7-year period to ever go through each box at some point during their advection. Areas without boxes contain less than 1% of the particles advected

overall distribution of materials away from the shelf break. Lastly, figure 4.3 demonstrates that a small percentage of all the particles released arrive inshore (1.5% of all particles). While there exists an area of slightly higher percentages to the southeast of CSG, the percentages in this area are less than 5%.

The particle density maps exhibit considerable interannual variability in their distribution of the number of particles that are advected away from the shelf break (figure 4.4). In particular, the tongue of higher particle density to the south of St. George Island varies in magnitude and extent each year, with 2005 and 2010 exhibiting the highest percentages of particles in this region. The strong el Niño year of 2010 contains a high number of particles

that reach well into the BBR and along the easternmost portion of the domain. This is the only year where particles are spread over nearly the entire BBR, particularly along the mid-shelf to the southwest of Cedar Key. This region to the south of Cedar Key is generally void of particles during years 2004-2009, giving credence to its colloquial name of the "Forbidden Zone, " as described by Yang et al. (1999). The onshore tongue of higher particle densities to the southeast of CSG is significantly diminished in all other years from the levels seen in 2005 and 2010. During other years, the percentage of particles that are advected inshore along the barrier islands of St. George Sound are less than 5%. In 2007, a moderate yet more widely-spread tongue of higher particle density is observed in this area with levels slightly higher than other years, although not quite approaching those observed in 2005 and 2010. These years with increased tongues of particle density are consistent with the years when the cross-shore flow features were enhanced in figure 3.15. In particular, the width and the strength of the onshore-flowing currents in the mean velocity fields are larger in years when higher number of particles traveled through these areas. Regardless of the percentage of particles that pass through this region to the southeast of CSG, it is clear that is an area where particles prefer to travel when being advected away from the shelf break.

4.5 Application to gag grouper larvae

The discussion of transport mechanisms in section 4.2 provides a simple assessment of the physics governing how materials are able to move across-isobath. What remains to be addressed is the pathways through which particles travel if they are able to reach areas of the domain corresponding to favorable juvenile gag nursery habitats. Therefore, the ability of passive Lagrangian particles to arrive inshore will determine if the physical mechanisms described in section 4.4 can provide the onshore transport necessary for gag larvae.

By examining the spatial density of only those particles who successfully reach within the 10m isobath at some point during their advection, the primary pathways for onshore transport may be elucidated. The 10m isobath is chosen as the nearshore region for this study, as it provides a rough estimate of where seagrasses may occur in the BBR. While seagrasses may not be extremely abundant at depths of 10m, it may also be assumed

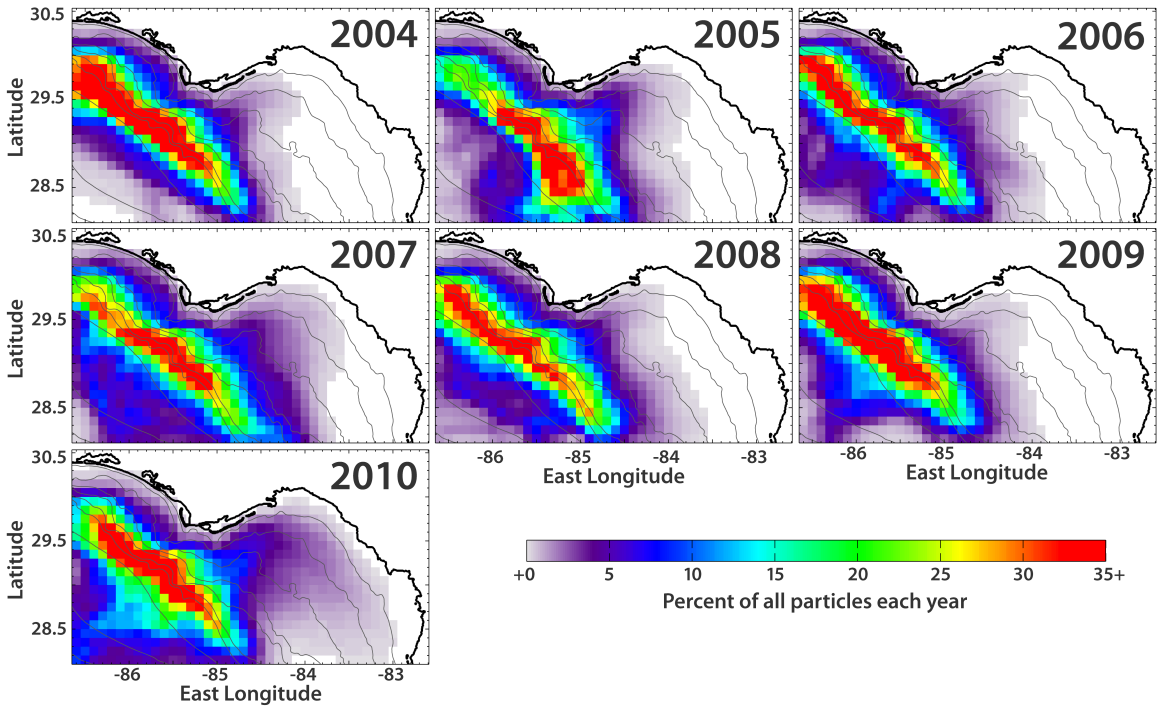

Figure 4.4: Same as figure 4.3, except separated for each year using the CFSR-forced BBROMS simulation and LTRANS.

that inshore of this isobath, other processes such as tides and buoyant river plumes play a more prominent role in governing local flow features. Indeed, it was suggested by Keener et al. (1988) that the flow features that govern both the advection and the behavior of gag in the nearshore region may differ from those during their advection offshore and over the shelf. Thus, the 10m isobath is considered the transition to the nearshore region. Figure 4.5 demonstrates the particle density for only those particles that arrive within the 10m isobath at some point during their advection (henceforth referred to as "successful" particles). The highest percentage of successful particles pass through the area immediately to the south of CSB and CSG, with percentages near or greater than 60%. This area is the same area where slightly higher tongues of particle density were observed in figure 4.4 (for 2005 and 2010) and is an area that exhibits significant onshore flow in the mean circulation (figure 3.12). It is interesting to note that, of all these successful particles, very few travel to the south of about 28.8^{o}N either during their time along the shelf break or when being advected

along the southeastward-flowing coastal jet. This demonstrates that the primary pathway by which particles are able to reach inshore is via the region just south of CSG, where there are two areas of onshore-directed mean velocities. Furthermore, the "Forbidden Zone" is potentially known as such because the geometry of the region simply does not allow the flow to carry shelf-break particles far enough south during these oscillatory winds. Only during 2010 are particles able to reach this far south along the coast.

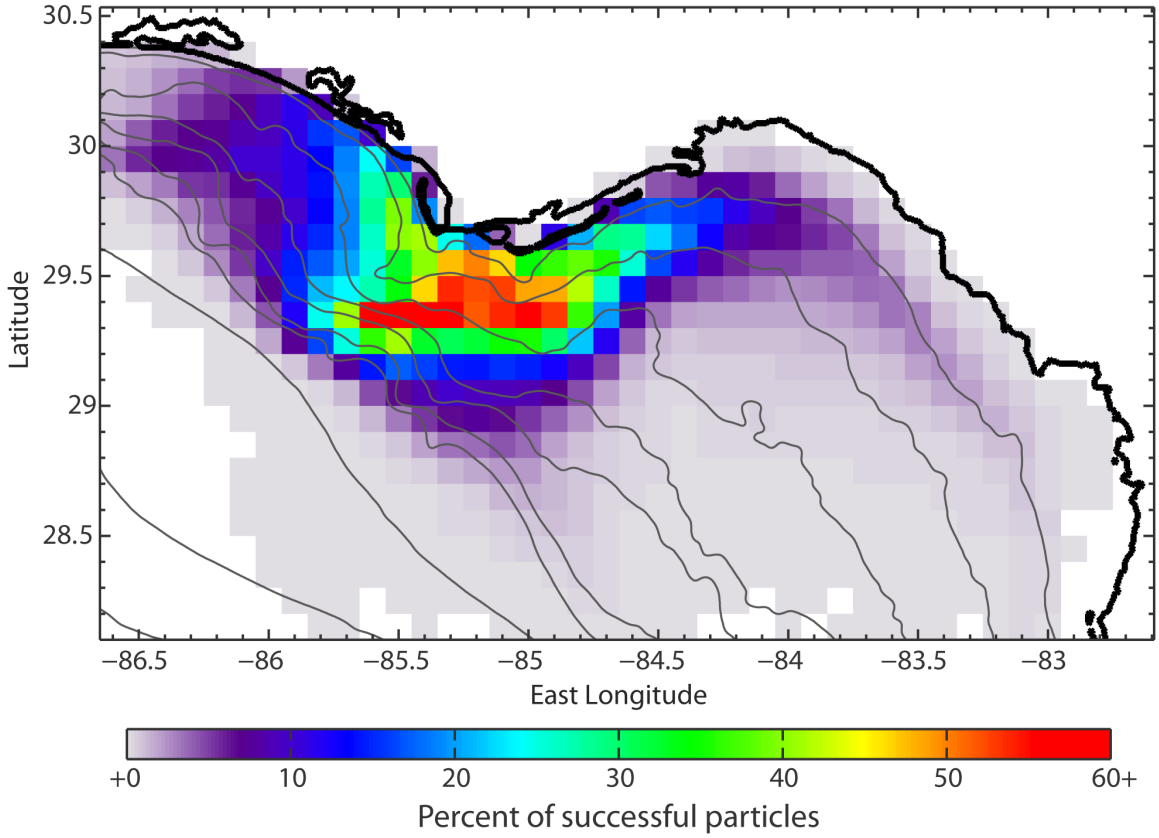

Figure 4.5: Same as figure 4.3, except only for particles who successfully reach the 10m isobath during their advection.

Since very few successful particles travel south of 28.8°N during their advection, it poses the question of whether particles originating along the southern parts of the BBR shelf break are even capable of reaching the nearshore environment. That is, in addition to identifying the primary pathways by which particles arrive at the 10m isobath, it is also of interest to consider where these successful particles originate. This will facilitate the understanding of

whether or not there are preferred spawning locations for particles based on the major flow features of the region.

There exist 156 seeding locations along the shelf break in the BBR (figure 2.1). The origins of successful particles may be traced in order to estimate the percentage of particles originating from each location that successfully reach the 10m isobath. This analysis reveals that the highest percentage of particles to arrive inshore originate to the south of CSB, in the region of tightly curving isobaths and where significant cross-shore velocities are visible in the mean (figure 4.6). Coincidentally, this is also adjacent to the region of highest successful particle density, and the locations with the closest proximity to the coast. In this area, about 10% of all the particles released arrive inshore of the 10m isobath at some point during their advection. So, while only 1.5% of all the particles released from all locations arrive inshore, the number of successful particles come predominantly from this area offshore of CSB. In fact, particles released to the south of 28.8^oN or to the west of 86.1^oW are largely unsuccessful at reaching the nearshore region (less than 1% of all particles originating here are successful). This region where the highest percentage of successful particles originate also coincides with a known gag spawning aggregation site (the Madison Swanson Marine Reserve; Koenig et al. 2000). The co-location of the preferred release locations with a known gag spawning aggregation suggests that this area could be selectively chosen by gag as a spawning site due to its geographic proximity to areas where materials are preferentially transported into the suitable seagrass nursery habitats of the BBR.

4.6 Summary

It has been demonstrated through the use of simple physical concepts and by use of Lagrangian particle advection model, that the mean cross-shelf velocities observed in figures 3.12-3.14 exist due to the rectification of flow during two dominant wind regimes that conserve their potential vorticity while flowing over tightly curving isobaths. The ocean's response to the large-scale, low-frequency wind forcing is barotropic and governed by the conservation of PV, which allows for cross-isobath flow during northwesterly winds and along-isobath flow during southeasterly winds. Stronger flow during winds from the northwest causes a higher Rossby number, and thus provides more potential for cross-shore

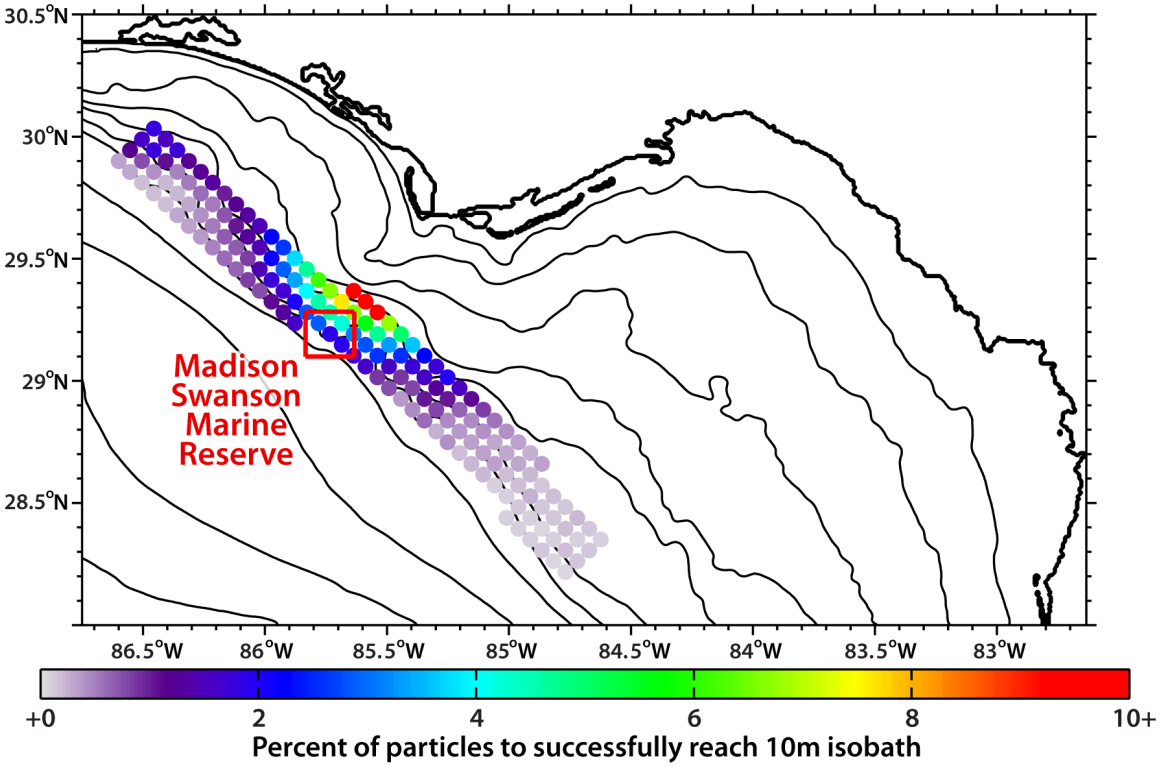

Figure 4.6: Dots denote the particle seeding locations, and are colored based on the percentage of all particles released from each location that successfully reach the 10m isobath at some point during their advection period. The total number of particles originating from each seeding location is 9,408.

movement. Through the conservation of PV, this strong flow is required to turn in the offshore (onshore) direction by adding negative (positive) relative vorticity as a response to quickly encountering shallower (deeper) isobaths. Consistent with this theory, the flow during southeasterly winds is weaker and therefore the potential for cross-shore movement is reduced. Therefore, the flow quickly adjusts to changing depths and it tends to follow isobaths.

Most particles released along the shelf break in the springtime circulation never reach areas that are suitable habitats for juvenile gag survival. Particles are primarily advected along the shelf break and toward the northwest, in association with the slope jet flowing in this direction. However, consistent with PV conservation, some particles are able to move across-isobath and onshore during northwesterly wind events. It is the areas of significant

cross-shore velocities described in detail in the previous chapter that provide the conduit for this onshore transport. This is evident from the successful particle density maps, which indicate that the primary pathway by which particles are able to reach inshore is immediately to the south of St. George Island, and north of 28.8^{o}N. The particle density maps also indicate that a significant amount of interannual variability occurs in the percentage of particles that are able to reach this preferred onshore pathway to the south of St. George Island. In particular, the strong el Niño year of 2010 exhibits an much higher percentage of particles that are capable of reaching the nearshore region of the BBR.

The existence of preferred particle seeding locations in close proximity to a known gag spawning aggregation site leads to many important implications that the dominant flow features provide to the biological species of interest. In particular, it could be assumed that the location of such a prominent origin for successful particles could be utilized by the biology in order to increase the percentage of larvae that successfully make it to the nursery habitats. Since greater than 10% of the particles advected in this location over the 7-year period may make it to the nearshore environment, it suggests that this location is preferentially chosen based on the ability of materials to arrive inshore from this area. Furthermore, there is now evidence that the two distinct zoographic regions of gag along the WFS outlined by Fitzhugh et al. (2005) could be simply set by the physical mechanisms that are capable of providing the transport onshore for these larvae. While the southern WFS region or the Yucatan region described by Fitzhugh et al. (2005) are not addressed in this study, it is likely that there are different physics governing the onshore flow further south, as the wide shelf does not experience many regions of tightly curving isobaths.

CHAPTER 5

SUMMARY AND CONCLUSIONS

5.1 Summary of the work

The BBR of Florida is an ecologically diverse and geometrically unique region in the Northeastern Gulf of Mexico. The unique geometry of the BBR contributes to the dominant flow features observed during the springtime. Previous studies of the region have demonstrated that there is a demand for a 4-dimensional approach toward understanding the major flow features in the BBR. Furthermore, ecologists have indicated a desire to understand how these flow features contribute to onshore transport and therefore to the dispersion of gag grouper larvae. However, observational studies in the region have either been sparse in time or limited in their spatial applicability. Thus, in order to fill this void in spatial and temporal coverage, this study uses several contemporaneous high-resolution ocean model simulations for the period 2004-2010 to describe the dominant flow features and primary transport mechanisms on the BBR shelf. Four different atmospheric datasets of varying spatial and temporal resolution are used to force the contemporaneous simulations, allowing for an analysis of how differing the atmospheric representation manifests itself in the ocean circulation.

It is found that the ocean responds to large-scale, low-frequency winds and not to smaller temporal or spatial scale variations in the winds. All atmospheric products reproduce low-frequency winds that have peaks in their power spectra near the same frequencies (4.386 $\pm$ 0.747 days), and as such the differences between the resulting 7-year mean circulations are small. The main flow features of the 7-year mean springtime BBR circulation include a northwestward-flowing slope jet, a southeastward-flowing coastal jet, and several areas of

cross-shelf velocities offshore of CSB and CSG. These cross-shelf velocities in the mean form a banded structure of offshore-directed velocities adjacent to onshore-directed velocities. The slope jet flow toward the northwest is set primarily by the deep ocean, but the flow on the shelf is set by the large-scale, low-frequency wind stress.

The hydrodynamic fields from the ocean model simulations are compared to several observations across the region, which include two current profiler time series at separate sites in 19m depth, three coastal sea level gauges, three surface temperature sensors at regional buoys, and satellite surface temperature observations. The model simulations all reproduce sea levels and surface temperatures that closely match observations at tide gauges ($R > 0.8$) or regional buoys ($R > 0.96$), respectively. When comparing modeled velocities to observed velocities at two different current meters located in depths of 19m, the models generally capture the variability of sub-inertial velocities at both sites well ($R > 0.7$). The exception to this generally good agreement is for the NARR-forced run, which performs poorly at capturing the variability seen in the observed curents. This is found to result from a systematic weak bias in the NARR winds. Therefore, even though this run captures the mean features well, its variability does not match that of the observed currents.

The mean circulation in the BBR is composed almost entirely of flow during two opposing wind regimes: winds from the northwest and winds from the southeast. Winds from easterly quadrants are much more frequent during the spring months, but northwesterly winds are stronger. These stronger, yet less frequent, northwesterly winds drive a correspondingly strong southeastward flow that is able to cross isobaths over regions where the isobaths exhibit tight curvature. Contrastingly, the flow during southeasterly winds is more frequent, but generally weaker. This weaker flow is able to more closely follow isobaths as it flows towards the northwest. The rectification of these two asymmetric, yet opposite oscillating flows provides a mean flow that is directed cross-shore in the regions of tightly curving isobaths, and relatively weak elsewhere.

It is shown that simple shallow-water conservation of potential vorticity governs the flow over the BBR shelf. The flow over the shelf is seen to respond barotropically to the winds. Lagrangian particles advected in the circulation demonstrate that the flow responds to changing ocean depths by inducing a change in relative vorticity of equal sign

and magnitude. This indicates that, following PV conservation, the flow is able to cross isobath during northwesterly winds, as the strong flow quickly encounters shallower (deeper) depths and is forced to turn to the right (left) in the offshore (onshore) direction in order to add a compensating negative (positive) relative vorticity. Flow from the southwest, on the other hand, is weaker and able to quickly adjust to changing isobaths without the need to induce much relative vorticity.

The Lagrangian particle trajectories also reveal the primary pathways that particles follow during their advection in the springtime circulation. Higher particle densities along the shelf break reveal that the primary pathway for advection is along the northwest-flowing slope jet, with advection away from the shelf break occurring due to the cross-isobath flow during northwesterly winds. There is considerable interannual variability in particle density patterns, particularly in the extent across the shelf that particles are able to reach. However, the cross-isobath movement is limited, and only a small percentage of particles are able to make significant progress insohre. The years that exhibit higher percentages of particles advected away from the shelf break correspond to years when the strength and width of mean cross-shore current features are larger.

A primary pathway for advection for particles that are successfully able to reach the nearshore region exists to the south of St. George Island, where over 60% of successful particles travel at some point during their advection. This indicates that successful particles are carried inshore by way the cross-shore currents offshore CSB and CSG and via the coastal jet. Significant interannual variability also occurs in the number of particles that arrive in this region of higher successful particle density. There are significantly more particles that follow this onshore tongue in 2010, indicating that the strength of el Niño phases (2010 was a strong el Niño year) could have a considerable impact on the magnitude of cross-shore transport in the BBR.

Lastly, and perhaps most interestingly (from a biological perspective), there exists a preferred origin for successful particles to the southwest of CSB. This preferred area of particle origins is immediately adjacent to the ara of high successful particle density, the regions of mean cross-shore currents, and a known gag spawning site, the Madison Swanson Marine Reserve (MSMR). The location of this preferred origin for successful particles has

many interesting implications, including whether or not gag have chosen this site as a preferred spawning site due to the increased ability for materials originating from this area to arrive inshore. This, along with some other implications of the work, will be discussed next.

5.2 Conclusions of the work

This work, for the first time, provides a complete description of the mechanisms capable of providing transport from the shelf break to the nearshore portions of the BBR from a full 4-dimensional perspective. In addition, it is the first successful attempt at describing how the physical ocean circulation plays an important role in setting the transport from adult gag spawning grounds to juvenile gag nursery habitats. A 4-dimensional approach toward understanding the physical circulation features that contribute to the onshore transport of gag larvae is demanded by Fitzhugh et al. (2005), as they find a simple empirical model to be insufficient. Furthermore, Weisberg and He (2003) use a 4-dimensional approach to describe the flow features, and indicate that the flow could be important to larval advection, but they never address the transport explicitly.

This work also reiterates the importance of the MSMR as a spawning aggregation site, except in a completely novel view. The establishement of the MSMR provided an area where fishing pressure on gag could be reduced, as fish species that form spawning aggregations and those that change sex are much more susceptible to overexploitation (as is the case for all shallow-water groupers; Coleman et al. 1996; Koenig et al. 2000). However, this work suggests that this reserve is also an important area because it is a preferred source region for transport into the shallow waters of the BBR. Therefore, the existence of preferred particle origins near MSMR suggests that this location could have been evolutionarily chosen as a spawning aggregation site because it provides shelf-break spawning gag with the highest chance for their offspring to survive and therefore sustain their population.

It is interesting to note that the one very strong el Niño year covered over the study period for this dissertation has a very different circulation and particle transport signature from the other six years. While this study period is too short to make any definitive conclusions about the impact of the ENSO phase on the flow characteristics, there is some

evidence that strong positive ENSO phase (el Niño) could lead to increased onshore transport. The other two years with increased levels of onshore transport (2005 and 2007) are also moderate el Niño years, although all other years are either near-neutral or negative ENSO phase (la Niña), and their circulation and transport patterns are more comparable. Since ENSO phase is negatively correlated with 500 hPa heights over the southeast United states (Hoerling and Kumar 2001) and positively correlated with precipitation over the same region (Ropelewski and Halpert 1986), the southeast United States often experiences colder, stormier winters in association with el Niño. This implies more cold front passages during el Niño, and hence more frequent northwesterly winds. Therefore, it is feasible to assume that positive ENSO phase could lead to increased success of gag larvae in the BBR, as the more frequent northwesterly winds during el Niño years provide ocean currents with a higher potential for cross-shore movement.

Sampling efforts in the eastern GOM indicate that juvenile gag are found along the entire WFS, and not just in the BBR. Fitzhugh et al. (2005) distinguish those gag found further south along the WFS to be zoographically different, as they arrive inshore at different times and different locations. This dissertation does not assess the advection of particles south of 28^{o}N, and so the applicability of these results to the advection of gag larvae along the southern portions of the WFS is unclear. It is found that 5-10% of particles originating to the southwest of CSB are capable of reaching inshore by way of passive advection alone. However, the dominant cross-shore transport mechanisms in the BBR are reliant on the unique bathymetry of the region. Further south along the WFS, the isobaths exhibit much less dramatic curvature and experience no significant bends in the isobaths along the shelf break until the southernmost part of the WFS near the Florida Keys. Furthermore, the southward extent of cold fronts is limited, and the southern portions of the WFS may not experience the same post-frontal wind speeds as those observed over the BBR. Therefore, it is quite possible that the physical mechanisms capable of providing cross-shelf transport over the WFS are vastly different from the BBR.

This work motivates the need for empirical sampling efforts for gag larvae. It has been documented (i.e. Keener et al. 1988) that gag have not been found to be among those species identified from decades of icthyoplankton surveys in the Gulf of Mexico. With the

information provided in this dissertation, primarily that onshore movement is possible to the south of St. George Island during northwesterly winds, sampling efforts may be focused in space and time to improve the possibility of capturing gag larvae. This will hopefully provide a clearer understanding of the behavior of gag larvae during their time of ingress, and thereby lead to an improved model for larval advection that includes behavior.

5.3 Future work

This section addresses some of the future work to be added as a follow-up to this research, and to provide an understanding of some of the additional steps that may be taken in order to reach the broad goal of being able to properly and effectively manage the BBR gag fishery.

First, this work has not addressed the affect that the biology may have on the physical advection inshore. It is very likely that gag larvae exhibit some distinct behavior during their development into juveniles. Larval behavior depends on many environmental factors, such as food availablity, mortality, predation, and sensitivity to changes in temperature and salinity (Cushing 1975, 1990; Norcross and Shaw 1984; Colin et al. 1996; Werner et al. 2007). A conceptual model for potential gag larval behavior can be made in order to test the impact that biological behavior has on the overall distribution of particles across the shelf. While it is noted that the behavior is unknown, a conceptual model for the behavior may be based on behavior of similar species and using the limited infomation that is known about this larval developmental stage of their life (e.g. Colin et al. 1996). In light of this, some simple LTRANS runs have been completed with very basic larval behavior. These include surface-following particles, bottom-following particles, diel vertical migration, and reverse diel vertical migration. While these behaviors are extremely simplified, analysis of these particle advection experiements will contribute to the discussion of the importance that biological behavior may have on modifying the transport inshore.

This work also excludes tides as a forcing mechanism of the shelf circulation. As work progresses in this interdisciplinary field, it would be of interest to assess the role of tidal forcing in setting potential particle displacements. While the tides have been shown to be fairly weak in the GOM (He and Weisberg 2002a), they could be potentially used by

the biology in the nearshore region. Keener et al. (1988) demonstrated that pre-settlement juveniles relied on the tides for their influx through the barrier islands off the coast of South Carolina. In light of their work, it is possible that gag could exhibit a very similar behavior in the BBR when reaching the nearshore environment, where tides may have a more prominent role. However, assessment of the role of tides is only possible if model simulations are completed with tides included as a forcing mechanism to the shelf circulation.

This study assesses the forward progress of particles originating at the shelf break. Since the particle displacements are estimated in LTRANS based on the modeled circulation, it is also possible to track the backward progress of particles that have arrived inshore. That is, particles may be seeded along the 10m isobath in the BBR, and traced backward in time in order to have a better understanding the origins and pathways of particles who reach the 10m isobath along the entire BBR. This will aid in the understanding of mechanisms that are capable of providing onshore transport to the southern portion of the BBR near Cedar Key.

Finally, this work can be put in the context of a seasonal or climate-scale modeling approach. In the previous section, it is mentioned that ENSO phase might have an important role in setting the amount of onshore transport that is possible in a given year. However, in order to understand the role that ENSO phase has on the circulation and transport characteristics, it is necessary to have enough years of model simulations to capture several ENSO cyles. There is much recent discussion in the physical science community about the impact that global climate change may have on not only the circulation and water mass properties, but also on ecologial systems. Thus, by using a down-scaled model in association with long-term (climate-scale) predictions, it is possible to assess how transport characteristics in the BBR might vary under forcing that undergoes climate change scenarios.

In the end, every step that is taken toward improving the knowledge of gag life cycle will lead to better management of the fisheries. In order to protect and maintain the gag fishery as a sustainable and valuable resource, it is essential that its management is done with the best knowledge of population variability. This study contributes to that knowledge by identifying the primary pathways by which the circulation alone is capable of providing the necessary transport onshore, and the mechansims by which these pathways

exist. However, much more can be learned about this early life cycle of gag. The iterative process of interdisciplinary research will only add to that knowledge. It is the hope of the author that interdisciplinary work continues in this field, so that this valuable economic and ecological resource may be sustained.

APPENDIX A

DESCRIPTION OF THE BBROMS MODELING FRAMEWORK

A full description of BBROMS numerics, grid specifications, and forcing is provided in this Appendix. First, a description of the numerical schemes is presented, followed by a detailed description of grid choice. Then, a comprehensive discussion of the model forcing fields and their application is given.

A third order, upstream-biased advection scheme is used for momentum, implemented with a specifically designed predictor-corrector time step algorithm. This allows the generation of physically-realistic steep gradients (Shchepetkin and McWilliams 1998). Advection of tracers is computed using the multidimensional positive definite advection transport algorithm (MPDATA), which reduces numerical overshoots and spurious diapycnal mixing by use of a flux-corrector scheme (Smolarkiewicz 1984). A splines density Jacobian is used for calculation of the horizontal pressure gradient (Shchepetkin and McWilliams 2003), and the Mellor Yamada 2.5 turbulence closure scheme is used with improvements from the Kantha and Clayson stability function (Mellor and Yamada 1974, 1982; Kantha and Clayson 1994).

The BBRROMS is configured for a rectangular-shaped domain with constant $1/120^o$ horizontal grid-spacing. The domain spans roughly 400 km in the zonal direction and 281.5 km in the meridional direction, making a horizontal grid of 500 x 305 cells. The BBROMS has 30 vertical, terrain-following, s-coordinate levels, with stretching parameters defined using the formulae

$$z(x,y,\sigma,t) = \zeta(x,y,t) + [\zeta(x,y,t) + h(x,y)]\, S(x,y,\sigma) \tag{A.1}$$

$$S(x,y,\sigma) = \frac{h_c\sigma + h(x,y)C(\sigma)}{h_c + h(x,y)} \tag{A.2}$$

where $S(c, y, \sigma)$ is a nonlinear vertical transformation functional, $\zeta(x, y, t)$ is the time-varying free-surface, $h(x, y)$ is the unperturbed water column thickness ($z = -h(x, y)$ corresponds to the ocean bottom), σ is a fractional vertical stretching coordinate ranging from $-1 \leq \sigma \leq 0$, $C(\sigma)$ is a non dimensional, monotonic, vertical stretching function ranging from $-1 \leq C(\sigma) \leq 0$, and $h_c = 100$ is a positive thickness controlling the stretching (see www.myroms.org). It is important to note that

$$S(x, t, \sigma) = \begin{cases} 0, & \text{if } \sigma = 0, \quad C(\sigma) = 0, \quad \text{at the free-surface;} \\ -1, & \text{if } \sigma = -1, \quad C(\sigma) = -1, \quad \text{at the ocean bottom;} \end{cases} \tag{A.3}$$

which allows the the stretching to behave like an equally-spaced sigma-coordinate in shallow regions where $h(x, y) << h_c$. The vertical stretching functions, $C(\sigma)$ are defined as a continuous, double stretching function:

$$\text{Surface Refinement function:} \quad C(\sigma) = \frac{1 - \cosh(8\sigma)}{\cosh(8) - 1} \tag{A.4}$$

$$\text{Bottom Refinement function:} \quad C(\sigma) = \frac{e^{4C(\sigma)} - 1}{1 - e^{-8}} \tag{A.5}$$

The result is a stretching of the vertical grid that has enhanced resolution near the surface and the bottom, with nearly uniform stretching in shallow waters.

Bathymetry for the BBROMS model is provided by the 30 arcsec Digital Elevation Model (DEM) from the National Geophysical Data Center (NGDC). The DEM grid-spacing matches exactly that of the BBROMS. In order to satisfy grid-stiffness parameters and to reduce the potential for the generation of spurious mixing, the bathymetry is globally smoothed using Gaussian weighted average with a radius of 3 grid cells. Then, areas of enhanced grid-stiffness (rx1 and rx0 defined by Haney 1991; Beckmann and Haidvogel 1993; respectively) are subjectively filtered using 9-point average over the region of enhanced grid-stiffness. Near the boundaries, the bathymetry is relaxed toward bathymetric values used by the GOM HYCOM with a relaxation function (described below for the boundary conditions). This relaxation of the the model bathymetries toward HYCOM's bathymetry allows the boundary conditions from HYCOM to be as consistent as possible across the boundary.

The initial conditions for the BBROMS simulations are provided by the GOM HYCOM. HYCOM's diagnostic output files are provided at standard Levitus depth levels and archive files are output as daily snapshots at 0 UTC. BBROMS initial fields for temperature, salinity, sea level, barotropic velocities, and full horizontal velocities are extracted from the GOM HYCOM time series at 0 UTC on 1 Jan 2004. Since the standard Levitus depth levels may not extend to the sea floor at all locations across the domain, the 3D HYCOM fields (temperature, salinity, and horizontal velocities) are filled downward from the shallowest valid depth. Then, all fields that have been land-masked are filled with the closest ocean value along a column or row at each depth. Finally, all HYCOM output fields are linearly-interpolated in the horizontal to the BBROMS C-grid, then interpolated in the vertical to the BBROMS initial depth levels using splines. Ocean model hindcast simulations are run continuously for the period 2004-2010, a hindcast period that is overlapped by juvenile gag collection efforts in the BBR. Adjustment from the initial conditions and equilibrium with the surface forcing occurs in about two weeks from model start, and is in relative balance well before 01 Feb 2004.

The model's open boundary conditions for temperature, salinity, sea level, barotropic velocities, and full horizontal velocities are prescribed using output from the the GOM HYCOM. The fields are interpolated to the initial BBROMS depth levels using the same technique described for the initial conditions. The interpolated GOM HYCOM fields are then imposed using radiation conditions at the open boundaries and with a nudging term that is imposed at the boundary and over a transition zone near the boundary (Marchesiello et al. 2001; Barth et al. 2008). This provides a relaxation of the flow features in this transition zone near the boundary toward those values specified by the GOM HYCOM. This essentially specifies the final prediction of the model field to be a weighted combination of the intially predicted BBROMS field and the field set by the GOM HYCOM. For example, the equation for any of the predicted fields has a term such as:

$$\frac{\partial A}{\partial t} = \ldots + T_{\text{nudge}} \left(A - A_O \right) \tag{A.6}$$

where A is the predicted value of temperature, salinity, sea level, or velocity from BBROMS, A_O is the corresponding field from the GOM HYCOM, and T_{nudge} a relaxation time scale

that follows the formula

$$T_{\text{nudge}} = \begin{cases} (1/\tau)\, e^{-x/15} & \text{for } x \leq 46 \\ 0 & \text{elsewhere} \end{cases} \tag{A.7}$$

where $\tau = 0.1$ days and x is the number of grid cells away from the boundary. T_{nudge} ranges from a relaxation time scale of 0.1 days at the boundary to 10 days at 44 grid cells inshore of the boundary. For this region, 46 grid cells roughly corresponds to the upper range of the internal radius of deformation, a length scale assumed to preserve significant features propagating into the region through the outer boundary. In addition to this flow relaxation, Flather boundary conditions are applied at the open boundary to the two-dimensional momentum variables normal to the boundaries, and Chapman boundary conditions are applied to the free surface to allow for gravity wave radiation at the open boundary (Flather 1976; Chapman 1985).

The ocean model uses 10m winds, air temperature, specific humidity, pressure, rainfall, and short- and long-wave radiation from the atmospheric products described in section 3.2.2 to calculate momentum, heat, and freshwater fluxes from bulk formulae (for description of the COARE 3.0 algorithm see Fairall et al. 2003). Model runs forced with CFSR, NARR, and NOGAPS use the downward longwave radiation provided by each dataset, and the upward longwave flux is calculated using the BBROMS surface temperatures. However, since the downward-only variables are not available for the Central America configuration of COAMPS, the COAMPS-forced BBROMS uses net longwave radiative fluxes from the atmospheric model to which a +20 W/m^2 bias correction is added. This is done to adjust for cold surface temperature bias that is observed using the COAMPS forcing with standard net longwave radiation. A test run was completed in which all COAMPS fields were provided as atmospheric forcing, with the exception of a downward longwave radiation provided from the NOGAPS instead of the net longwave radiation from COAMPS. The resulting circulation provided an SST that qualitatively matched the other modeled SSTs and satellite SSTs. By adding a +20 W/m^2 correction to the COAMPS longwave radiation field, the estimate of the SSTs is improved when compared to the other modeled and satellite-observed SSTs. All runs use the net shortwave radiation provided from their respective atmospheric forcing product.

Nineteen different rivers are prescribed as fluxes of momentum and low salinity water at the coast. The simulated rivers included in the BBROMS configuration are the Apalachicola, Aucilla, Carabelle (aka "New River"), Chassahowitzka, Choctawhatchee, Crystal, Fenholloway, Homosassa, Ochlockonee, Pithlachascotee, Sopchoppy, St. Mark's, Steinhachee, Suwannee (East and West Pass), Waccasassa, Weeki Wachee, and Withlacoochee Rivers, and Econfina and Spring Creeks. These rivers were chosen because of their location within the BBR and by the magnitude of their discharge. Indeed, there exist other rivers in the BBR that are excluded from this list, due to their comparatively small discharge. River outflows are prescribed using daily means from United States Geological Survey gauges, and are applied as constant sources of fresh water (3 PSU). River temperatures vary as monthly climatology values, and streamflows are applied as linear profiles in the vertical, following the formulation:

$$y = x/3 \tag{A.8}$$

where y = the percentage of the flow rate in that layer, x = the layer index ranging from 0–29. This linear profile of river outflow allows a higher percentage of outflow to occur at the surface.

APPENDIX B

FILTERING PROCEDURES FOR SUB-INERTIAL FLOW

This appendix describes the filtering procedures that are used for filtering both observational and model output data to obtain sub-inertial, or low-frequency flow. For all data with a significant tidal component (observed currents, observed sea levels), the lunar monthly and fortnightly tidal signals are removed as a first step by calculating a least squares fit to the function

$$x_f(t) = \mu + A(i)\cos(2\pi f t(i)) + B(i)\sin(2\pi f t(i)) \tag{B.1}$$

where x_f is the fitted signal, t is the time of observations, and the values of f are the frequencies of the lunar fortnightly tide, the lunar monthly tide, and the nonlinear interaction of the tide due to bottom friction: 13.6583, 27.554, and 14.7857 days, respectively. This long-period tidal signal is then removed from the data. Low-frequency tides are not subtracted from the modeled fields, as tides have not been prescribed as forcing for the model.

For all data that is being filtered for sub-inertial variability, a cosine-Lanczos filter is used (Emery and Thompson (2001)) following procedures outlined by Maksimova (2012), with a 'cutoff' frequency of 40 hours chosen for the filter. This passes 50% of the power at frequencies $2\pi/40$ hours and 10% at frequencies of $2\pi/30$ hours (Maksimova 2012). By using this procedure, variability is removed at frequencies shorter than 30 hours, resulting in sub-inertial (or low-frequency) variability of the flow.

APPENDIX C

DESCRIPTION OF THE LAGRANGIAN PARTICLE ADVECTION MODEL

This appendix describes the details of the Larval TRANSport Lagrangian Model (LTRANS; Schlag et al. 2008; North et al. 2006, 2008), which is the Lagrangian particle advection model used for this dissertation. LTRANS is configured to be run 'offline' using output from the BBROMS simulations. It uses a 4th order Runge-Kutta scheme to estimate particle movements due to velocities and a logarithmic reduction in current velocities within one s-level of the bottom. This is done in order to simulate a reduction in current velocities due to friction in the very near-bottom environment (North et al. 2006). In order to prevent the artificial aggregation of particles in regions of sharp diffusivity gradients, a smoothing algorithm is applied to the water column profile of vertical diffusivity (m^2 s^1), with values at the surface and bottom set to 0. This also satisfies the well-mixed criterion (North et al. 2006). Random walk is used to simulate turbulent particle motion in the horizontal direction.

For the particle advection experiments, 156 particles are seeded every 3 hours for 12 weeks from pre-determined release locations between the 50 and 100m isobaths (see figure 2.1), beginning at 00 UTC of 01 Feb each year. Passive particles are seeded at 0.5m below the surface and 0.5m above the bottom, and are free to move vertically in accordance with the flow. Each particle is followed for a maximum of 45 days, which corresponds to the mean gag pelagic larval duration.

Sea surface height, and hence water depth, are interpolated in space using bilinear interpolation. Current velocities, diffusivities, and salinity are interpolated in space using bilinear interpolation along s-levels in the horizontal and a tension spline in the z direction,

following a water-column profile scheme (North et al. 2006, 2008). Water properties are interpolated in time using a polynomial fit. Since there is no information of velocities outside of the model domain, particle trajectories are no longer followed once particles reach the open boundaries of the model domain. However, particles that intersect horizontal land boundaries are reflected off the boundary at a reflection angle equal to the angle at which each particle approaches to the boundary. Particles that pass through the surface or bottom boundary due to turbulence or vertical advection are vertically reflected back into the domain by a distance equal to the distance that the particle exceeded the boundary. In addition to the particle's horizontal and vertical position in the domain, the temperature and salinity at each particle location are recorded at an interval equal to the external time step of the model (3 hours).

REFERENCES

Barker, E., 1992: Design of the Navy's multivariate optimum interpolation analysis system. *Wea. Forecasting*, **7 (2)**, 220–231.

Barth, A., A. Alvera-Azárate, and R. H. Weisberg, 2007: Benefit of nesting a regional model into a large-scale ocean model instead of climatology: Application to the West Florida Shelf. *Cont. Shelf. Res.*, **28**, 561–573.

Barth, A., A. Alvera-Azárate, and R. H. Weisberg, 2008: A nested model study of the loop current generated variability and its impact on the West Florida Shelf. *J. Geophys. Res.*, **113 (C5)**.

Beckmann, A. and D. Haidvogel, 1993: Numerical simulation of flow around a tall isolated seamount. part i: problem formulation and model accuracy. *J. of Phys. Oceanogr*, **23**, 1736–1753.

Bleck, R., 2002: An oceanic general circulation model framed in hybrid isopycnic-cartesian coordinates. *Ocean Modelling*, **37**, 55–88.

Carlson, P., L. Yarbro, K. Kaufman, and R. Mattson, 2010: Vulnerability and resilience to hurricane and runoff impacts along Florida's West coast. *Hydrobiologia*, **649 (1)**, 39 – 53, doi:10.1007/s10750-010-0257-0.

Castelao, R. and J. Barth, 2006: The relative importance of wind strength and along-shelf bathymetric variations on the separation of a coastal upwelling jet. *J. of Phys. Oceanogr.*, **36**.

Chambers, R. and E. Trippel, 1997: *Early life history and recruitment in fish populations.* Chapman & Hall.

Chapman, D., 1985: Numerical treatment of cross-shelf open boundaries in a barotropic coastal ocean mode. *J. Phys. Oceanogr.*, **15**, 1060–1075.

Chassignet, E., 2011: Isopycnic and hybrid ocean modeling in the context of GODAE. *Operational Oceanography in the 21st Century*, A. Schiller and G. Brassington, Eds., Springer, 263–294.

Chassignet, E., H. Hurlburt, O. Smedstad, G. Halliwell, P. Hogan, A. Wallcraft, R. Baraille, and R. Bleck, 2007: The HYCOM (HYbrid Coordinate Ocean Model) data assimilative system. *J. Mar. Systems.*, **65**, 60–83.

Chassignet, E., et al., 2009: U.S. GODAE: Global ocean prediction with the HYbrid Coordinate Ocean Model (HYCOM). *Oceanography*, **22 (2)**, 64–75.

Clarke, A. and K. Brink, 1985: The response of stratified, frictional flow of shelf and slope waters to fluctuating large-scale, low-frequency wind forcing. *J. of Phys. Oceanogr.*, **15**, 439–453.

Clarke, A. and E. Maksimova, forthcoming: Seasonal subinertial Eulerian current observations near the Florida Big Bend coast. *J. of Phys. Oceanogr.*

Coleman, F., W. Figueira, F. Ueland, and L. Crowder, 2004: The impact of United States recreational fisheries on marine fish populations. *Science*, **305**, 1958–1959.

Coleman, F., C. Koenig, and L. Collins, 1996: Reproductive styles of shallow-water groupers (Pisces: Serranidae) in the eastern Gulf of Mexico and the consequences of fishing spawning aggregations. *Environmental Biology of Fishes*, **47**, 129–141.

Colin, P., C. Koenig, and W. Laroche, 1996: Development from egg to juvenile of the red grouper (*Epinephelus morlo*) (Pisles: Serranidae) in the laboratory. *Biology, fisheries and culture of tropical groupers and snappers*, F. Arreguin-Sánchez, J. Munro, M. Balgos, and D. Pauly, Eds., ICLARM Conf. Proc., 449 p., 48.

Continental Shelf Associates, I., 1997: Assessment of hurricane damage in the Florida Big Bend seagrass beds. Tech. Rep. 14-12-0001-30188, Mineral Management Service, New Orleans, LA.

Cummings, J. A., 2005: Operational multivariate ocean data assimilation. *Quarterly Journal of the Royal Meteorological Society*, **131 (613)**, 3583–3604.

Cushing, D., 1975: *Marine ecology and fisheries*. Cambridge University Press, 278 pp.

Cushing, D., 1990: Plankton production and year-class strength in fish populations: an update of the match/mismatch hypothesis. *Advances in Marine Biology*, **26**.

Dukhovskoy, D., S. Morey, and J. O'Brien, 2009: Generation of baroclinic topographic waves by a tropical cyclone impacting a low-latitude continental shelf. *Continental Shelf Research*, **29**, 333–351.

Emery, W. and R. Thompson, 2001: *Data Analysis Methods in Physical Oceanography*. 2d ed., Elsevier Science, 654 pp.

Fairall, C., E. F. Bradley, J. E. Hare, A. A. Grachev, and J. B. Edson, 2003: Bulk parameterization of air-sea fluxes: Updates and verification for the COARE algorithm. *J. of Climate*, **16**, 571–591.

Fitzhugh, G., C. Koenig, F. Coleman, C. Grimes, and W. S. III, 2005: Spatial and temporal patterns in fertilization and settlement of young gag (*Mycteroperca microlepis*) along the West Florida shelf. *Bull. of Mar. Science*, **77 (3)**, 377–396.

Flather, R., 1976: A tidal model of the northwest European continental shelf. *Memoires de la Societe Royale des Sciences de Liege*, **6 (10)**, 141–164.

Gaul, R., 1967: Circulation over the continental margin of the northeast Gulf of Mexico. Ph.D. thesis, Texas A & M University, 156 pp.

Gentemann, C. and Coauthors, 2009: MISST: The multi-sensor improved sea surface temperature project. *Oceanography*, **22 (3)**, 76–87.

Gentner, B., 2009: Allocation analysis of the Gulf of Mexico gag and red grouper fisheries. Tech. rep., Genter Consulting Group, Coastal Conservation Association, 27 pp.

Gilbes, F., C. Tomas, J. Walsh, and F. Mijller-Karger, 1996: An episodic chlorophyll plume on the West Florida shelf. *Cont. Shelf Res.*, **16 (9)**, 1201–1224.

Goerss, J. and P. Phoebus, 1992: The Navy's operational atmospheric analysis. *Wea. and Forecast.*, **7**, 232–249.

Gouillon, F., S. L. Morey, D. S. Dukhovskoy, and J. J. O'Brien, 2010: Forced tidal response in the Gulf of Mexico. *J. Geophys. Res.*, **115 (C10050)**.

Haney, 1991: On the pressure gradient force over steep topography in sigma coordinate ocean models. *J. of Phys. Oceanogr.*, **21**, 610–619.

He, R. and R. Weisberg, 2002a: Tides on the West Florida Shelf. *J. of Phys. Oceanogr.*, **32**, 3455–3473.

He, R. and R. Weisberg, 2002b: West Florida shelf circulation and temperature budget for the 1999 spring transition. *Cont. Shelf Res.*, **22**, 719–748.

He, R. and R. Weisberg, 2003: A case study of the Loop Current intrusion on the West Florida Shelf. *J. of Phys. Oceanogr.*, **33 (2)**, 465–477.

Hetland, R., Y. Hsueh, R. Lebe, and P. Niiler, 1999: A loop current-induced jet along the edge of the West Florida Shelf. *Geophys. Res. Letters*, **26 (15)**, 2239–2242.

Hodur, R., 1996: The Naval Research Laboratory's Coupled Ocean/Atmosphere Mesoscale Prediction System (COAMPS). *Mon. Wea. Rev.*, **125**, 1414–1430.

Hoerling, M. and A. Kumar, 2001: Atmospheric response patterns associated with tropical forcing. *J. Climate*, **15**, 2184–2203.

Hogan, T. F. and T. E. Rosmond, 1991: The description of the U.S. Navy Operational Global Atmospheric Prediction Systems spectral forecast model. *Mon. Wea. Rev.*, **119**, 1786–1815.

Hood, P. and R. Schlieder, 1992: Age, growth, and reproduction of gag, *Mycteroperca microlepis* (Pisces: Serranidae), in the easter Gulf of Mexico. *Bull. of Marine Sci.*, **51**, 337–352.

Iverson, R. and H. Bittaker, 1986: Seagrass distribution and abundance in eastern Gulf of Mexico coastal waters. *Estuarine, Coastal and Shelf Science*, **22**, 577–602.

Kantha, L. H. and C. A. Clayson, 1994: An improved mixed layer model for geophysical applications. *Journal of Geophysical Research: Oceans*, **99 (C12)**, 25 235–25 266.

Keener, P., G. Johnson, B. Stender, E. Brothers, and H. R. Beatty, 1988: Ingress of postlarval gag *Mycteroperca Microlepis* (Pisces: Serranidae), through a South Carolina barrier island inlet. *Bull. of Mar. Sci.*, **42 (3)**, 376–396.

Koenig, C. and F. Coleman, 1998: Absolute abundance and survival of juvenile gags in sea grass beds of the northeastern Gulf of Mexico. *Trans. of the American Fisheries Soc.*, **128**, 44–55.

Koenig, C., F. Coleman, C. Grimes, G. Fitzhugh, K. Scanlon, C. Gledhill, and M. Grace, 2000: Protection of fish spawning habitat for the conservation of warm temperate reef fish fisheries of shelf-edge reefs of Florida. *Bull. of Mar. Sci.*, **66**, 593–616.

Lemarié, F., J. Kurian, A. Shchepetkin, M. Molemaker, F. Colas, and J. McWilliams, 2011: Are there inescapable issues prohibiting the use of terrain-following coordinates in climate models? *Ocean Modelling*.

Lentz, S., 2012: Buoyant coastal currents. *Buoyancy-driven flows*, e. chassignet, c. cenedse, and j. verron, Eds., Cambridge university press, 164–202.

Li, Z. and R. Weisberg, 1999a: RWest Florida Shelf response to upwelling-favorable wind forcing: Kinematics. *J. Geophys. Res.*, **104 (C6)**, 13 507–13 527.

Li, Z. and R. Weisberg, 1999b: West Florida Shelf response to upwelling-favorable wind forcing: Dynamics. *J. Geophys. Res.*, **104 (C10)**, 23 427–23 442.

Liu, W. and W. Tang, 1996: Equivalent neutral wind. Tech. Rep. 96-17, JPL, 16 pp.

Maksimova, E. and A. Clarke, forthcoming: Multiyear subinertial Eulerian current observations near the Florida Big Bend coast. *J. of Phys. Oceanogr.*

Maksimova, E. V., 2012: Multiyear eulerian current observations near the Florida Big Bend coast. Florida State University, PhD Thesis, 68 pp.

Marchesiello, P., L. Debreu, and X. Couvelard, 2009: Spurious diapycnal mixing in terrain-following coordinate models: The problem and a solution. *Ocean Modelling*, **26 (3)**, 156–169.

Marchesiello, P., J. McWilliams, and A. Shchepetkin, 2001: Open boundary condition for long-term integration of regional oceanic models. *Ocean Modelling*, **3**, 1–20.

Marmorino, G., 1983: Variability of current, temperature, and bottom pressure across the West Florida continental shelf, Winter 1981-1982. *J. Geophys. Res.*, **8 (C7)**, 4439–4457.

Mellor, G. and T. Yamada, 1974: A hierarchy of turbulence closure models for planetary boundary layers. *J. of Atmos Science*, **31**, 1791–1806.

Mellor, G. and T. Yamada, 1982: Development of a turbulence closure model for geophysical fluid problems. *Reviews of Geophysics and Space Physics*, **20**, 851–875.

Mesinger, F. and Coauthors, 2006: North American Regional Reanalysis. *Bull. Am. Met. Soc.*, **87 (3)**, 343–360.

Meyers, S., E. Siegel, and R. Weisberg, 2001: Observations of currents on the West Florida shelf break. *Geophys. Res. Letters*, **28 (10)**, 2037–2040.

Mitchum, G. and A. Clarke, 1986: Evaluation of frictional, wind-forced long-wave theory on the West Florida shelf. *J. of Phys. Oceanogr.*, **16**, 1029–1037.

Mitchum, G. and W. Sturges, 1982: Wind-driven currents on the West Florida shelf. *J. of Phys. Oceanogr.*, **12**, 1310–1317.

Morey, S., D. Dukhovskoy, and M. Bourassa, 2009: Connectivity of the Apalachicola River flow variability and the physical and bio-optical properties of the northern West Florida shelf. *Cont. Shelf Res.*, **29**, 1264–1275.

Morey, S. and J. O'Brien, 2002: The spring transition from horizontal to vertical thermal stratification on a midlatitude continental shelf. *J. of Geophys. Res.*, **29**.

Morey, S., J. Zavala-Hidalgo, and J. O'Brien, 2005: The seasonal variability of continental shelf circulation in the northern and western Gulf of Mexico from a high-resolution numerical model. *Circulation in the Gulf of Mexico: Observations and Models*, Amer. Geophys. Union, No. 161 in Geophys. Monogr., 203–218.

Mullaney, J., M.D. and L. Gale, 1996: Ecomorphological relationships in ontogeny: anatomy and diet in gag, *Mycteroperca microlepis* (Pisces: Serranidae). *Copeia*, **1996 (1)**, 167–180.

Niiler, P., 1976: Observations of low-frequency currents on the West Florida shelf. *Mem. Soc. Roy. Sci. Liege*, **6**.

Norcross, B. and R. Shaw, 1984: Oceanic and estuarine transport of fish eggs and larvae: A review. *Trans. of the American Fisheries Soc.*, **113**, 155–165.

North, E., R. Hood, S.-Y. Chao, and L. Sanford, 2006: Using a random displacement model to simulate turbulent particle motion in a baroclinic frontal zone: A new implementation scheme and model performance tests. *J. of Mar. Science*, **60**, 365–380.

North, E. W., Z. Schlag, R. R. Hood, M. Li, L. Zhong, T. Gross, and V. S. Kennedy, 2008: Vertical swimming behavior influences the dispersal of simulated oyster larvae in a coupled particle-tracking and hydrodynamic model of Chesapeake Bay. *Marine Ecology Progress Series*, **359**, 99–115.

Ohlmann, J. and P. Niiler, 2005: Circulation over the continental shelf in the northern Gulf of Mexico. *Prog. in Oceanogr.*, **64**, 45–81.

Ropelewski, C. and M. Halpert, 1986: North American precipitation and temperature patterns associated with the el Niño/Southern Ooscillation (ENSO). *Mon. Wea. Rev.*, **114**, 2352–2362.

Rosmond, T., 1992: The design and testing of the Navy Operational Global Atmospheric Prediction System. *Weather and Forecasting*, **7**, 262–272.

Rothschild, B., 1986: *Dynamics of marine fish populations*. Harvard University Press, 277 pp.

Rothschild, B. and T. Osborn, 1988: Small-scale turbulence and plankton contact rates. *J. of Plankton Res.*, **10**, 465–474.

Saha, S. and Coauthors, 2006: The NCEP Climate Forecast System. *J. Climate*, **19**, 3483–3517.

Schlag, Z., E. W. North, and K. Smith, 2008: *Larval TRANSport Lagrangian model (LTRANS) User's Guide*. Cambridge, MD, University of Maryland Center for Environmental Science Horn Point Laboratory.

Shchepetkin, A. and J. McWilliams, 1998: Quasi-monotone advection schemes based on explicit locally adaptive dissipation. *Mon. Wea. Rev.*, **126**, 1541–1580.

Shchepetkin, A. and J. McWilliams, 2003: A method for computing horizontal pressure-gradient force in an oceanic model with a nonaligned vertical coordinate. *J. of Geophys. Res.*, **108**, 3090.

Shchepetkin, A. and J. McWilliams, 2005: The regional oceanic modeling system (roms): a split-explicit, free-surface, topography-following-coordinate oceanic model. *Ocean Modelling*, **9**, 147–404.

Smolarkiewicz, P. K., 1984: A fully multidimensional positive definite advection transport algorithm with small implicit diffusion. *J. Comput. Phys.*, **54**, 325–362.

Sturges, W., P. Niiler, and R. Weisberg, 2001: Northeastern Gulf of Mexico inner shelf circulation study. Tech. Rep. 14-35-0001-30787, Mineral Management Service, 90 pp., Herndon, VA.

Tolbert, W. and G. Salsman, 1964: Surface circulation of the eastern Gulf of Mexico as determined by drift-bottle studies. *J. of Geophys. Res.*, **79**, 223–230.

Weatherly, G. and D. Thistle, 1997: On the wintertime currents of the Florida Big Bend region. *Continental Shelf Research*, **17 (11)**, 1297–1319.

Weisberg, R., B. Black, and H. Yang, 1996: Seasonal modulation of the west Florida continental shelf circulation. *Geophys. Res. Letters*, **23 (17)**, 2247–2250.

Weisberg, R. and R. He, 2003: Local and deep-ocean forcing contributions to anomalous water properties on the West Florida shelf. *J. Geophys. Res.*, **108 (C6)**, 3184.

Weisberg, R., R. He, Y. Liu, and J. Virmani, 2005: West Florida shelf circulation on synoptic, seasonal, and interannual time scales. *Circulation in the Gulf of Mexico: Observations and Models*, Amer. Geophys. Union, No. 161 in Geophys. Monogr., 325–347.

Weisberg, R., Z. Li, and F. Muller-Karger, 2001: West Florida shelf response to local wind forcing: April 1998. *J. of Geophys. Res.*, **106 (C12)**, 31 239–31 262.

Werner, F., R. Cowen, and C. Paris, 2007: Coupled biological and physical models. *Oceanography*, **20**, 54–69.

Werner, F., J. Quinlan, B. Blanton, and R. L. Jr., 1997: The role of hydrodynamics in explaining variability in fish populations. *J. of Sea Res.*, **37**, 195–212.

Williams, J., W. Grey, E. Murphy, and J. Crane, 1977: Memoirs of the Hourglass cruises. report of the marine research laboratory. Tech. Rep. 3, Florida Department of National Research, 134 pp., St. Petersburg, FL.

Yang, H., R. Weisberg, P. Niiler, W. Sturges, and W. Johnson, 1999: Lagrangian circulation and forbidden zone on the West Florida shelf. *Cont. Shelf Res.*, **19**, 1221–1245.

Zetler, B. and D. Hansen, 1971: Tides in the Gulf of Mexico. *Contributions on the Physical Oceanography of the Gulf of Mexico*, Gulf Publishing, Vol. 2, 265–275.

BIOGRAPHICAL SKETCH

Austin grew up on the waters of the Chesapeake Bay in Annapolis, MD. In 2003, he began studies of Meteorology and Mathematics at Florida State University, receiving a double major in April 2007. The final year of his undergraduate studies, Austin performed research at the Florida State University Center for Ocean-Atmospheric Prediction Studies (COAPS), and established connections in the research field of Oceanography. Upon completion of his B.S., Austin pursued his interests in Physical Oceanography at FSU under the direction of COAPS director, Eric Chassignet. Austin's research interests lie in coastal ocean dynamics, numerical ocean modeling, and the influence of physical processes on coastal ecosystems.